Improved Simulation of Tropical Cyclone Responses to ENSO in the Western North Pacific in the High-Resolution GFDL HiFLOR Coupled Climate Model*

WEI ZHANG,[+,#,@] GABRIEL A. VECCHI,[+,#] HIROYUKI MURAKAMI,[+,#] THOMAS DELWORTH,[+,#] ANDREW T. WITTENBERG,[+] ANTHONY ROSATI,[+] SETH UNDERWOOD,[&] WHIT ANDERSON,[+] LUCAS HARRIS,[+] RICHARD GUDGEL,[+] SHIAN-JIANN LIN,[+] GABRIELE VILLARINI,[**] AND JAN-HUEY CHEN[+,#]

[+] *NOAA/Geophysical Fluid Dynamics Laboratory, Princeton, New Jersey*
[#] *Atmospheric and Oceanic Sciences Program, Princeton University, Princeton, New Jersey*
[@] *Collaborative Innovation Center on Forecast and Evaluation of Meteorological Disasters, Key Laboratory of Meteorological Disaster, Ministry of Education, and Earth System Modeling Center, Nanjing International Academy of Meteorological Sciences, Nanjing University of Information Science and Technology, Nanjing, China*
[&] *Engility Corporation, Chantilly, Virginia*
[**] *IIHR-Hydroscience and Engineering, The University of Iowa, Iowa City, Iowa*

(Manuscript received 6 July 2015, in final form 29 November 2015)

ABSTRACT

This study aims to assess whether, and the extent to which, an increase in atmospheric resolution of the Geophysical Fluid Dynamics Laboratory (GFDL) Forecast-Oriented Low Ocean Resolution version of CM2.5 (FLOR) with 50-km resolution and the High-Resolution FLOR (HiFLOR) with 25-km resolution improves the simulation of the El Niño–Southern Oscillation (ENSO)–tropical cyclone (TC) connections in the western North Pacific (WNP). HiFLOR simulates better ENSO–TC connections in the WNP including TC track density, genesis, and landfall than FLOR in both long-term control experiments and sea surface temperature (SST)- and sea surface salinity (SSS)-restoring historical runs (1971–2012). Restoring experiments are performed with SSS and SST restored to observational estimates of climatological SSS and interannually varying monthly SST. In the control experiments of HiFLOR, an improved simulation of the Walker circulation arising from more realistic SST and precipitation is largely responsible for its better performance in simulating ENSO–TC connections in the WNP. In the SST-restoring experiments of HiFLOR, more realistic Walker circulation and steering flow during El Niño and La Niña are responsible for the improved simulation of ENSO–TC connections in the WNP. The improved simulation of ENSO–TC connections with HiFLOR arises from a better representation of SST and better responses of environmental large-scale circulation to SST anomalies associated with El Niño or La Niña. A better representation of ENSO–TC connections in HiFLOR can benefit the seasonal forecasting of TC genesis, track, and landfall; improve understanding of the interannual variation of TC activity; and provide better projection of TC activity under climate change.

1. Introduction

Tropical cyclones (TCs) are among the most destructive natural hazards (Emanuel 2005; Pielke et al. 2008; Peduzzi et al. 2012; Zhang et al. 2009). The scientific community has paid considerable attention to the analysis of their genesis (Chia and Ropelewski 2002; Gray 1979; Zehr 1992; Gray 1998), track (Riehl and Shafer 1944; Fraedrich and Leslie 1989; Harr and Elsberry 1991; Dobos and Elsberry 1993; Holland and Lander 1993), landfall (Tuleya et al. 1984; Chan and Liang 2003; Lyons 2004), and intensity (Dvorak 1984; Chan et al. 2001; Emanuel et al. 2004; Wong and Chan 2004). Advances in the understanding of the physical and dynamical processes of TCs have been achieved with previous studies.

The El Niño–Southern Oscillation (ENSO) phenomenon plays an important role in modulating the statistics

* Supplemental information related to this paper is available at the Journals Online website: http://dx.doi.org/10.1175/JCLI-D-15-0475.s1.

Corresponding author address: Wei Zhang, NOAA/Geophysical Fluid Dynamics Laboratory, 201 Forrestal Road, Princeton, NJ 08540.
E-mail: wei.zhang@noaa.gov

DOI: 10.1175/JCLI-D-15-0475.1

of TC development, genesis, and track. ENSO arises from air–sea interactions in the tropical Pacific (Rasmusson and Carpenter 1982; Philander 1983; Cane and Zebiak 1985) and modulates weather and climate not only in the tropics but also the subtropics and extratropics by teleconnections (Wunsch 1991; Lau and Yang 1996; Lau and Nath 1996; Alexander et al. 2002). Mounting evidence has supported the influence of ENSO on TC genesis (Chan 1985; Wu and Lau 1992; Chan 2000; Wang and Chan 2002; Fudeyasu et al. 2006; Wang et al. 2007), intensity (Camargo and Sobel 2005; Chan 2008; Zhang et al. 2015), track (Wang and Chan 2002; Camargo et al. 2007; Hong et al. 2011; Li and Zhou 2012), and landfall (Wu et al. 2004; Fudeyasu et al. 2006; Zhang et al. 2012) in the western North Pacific (WNP) based on observations. For example, El Niño (La Niña) favors (suppresses) basinwide TC activity measured by accumulated cyclone energy in the WNP and enhances TC genesis in the southeastern (northwestern) portion of the WNP (Wang and Chan 2002; Camargo et al. 2005). More intense typhoons tend to occur during El Niño than La Niña because of the eastward shift in TC genesis and a longer time spent over warmer water and within a moister environment (Wang and Chan 2002; Camargo et al. 2005; Zhang et al. 2015). In addition, TCs are more likely to make landfall over East Asia during La Niña years because of a westward shift of TC genesis and of the subtropical high (Wu et al. 2004; Zhang et al. 2012). In contrast, there are more recurving TCs during the El Niño than the La Niña phase (e.g., Wang and Chan 2002; Hong et al. 2011). TC recurvature is a special type of TC track, turning from westward toward the north and eventually to the northeast in the Northern Hemisphere (Riehl and Shafer 1944; George and Gray 1977).

This connection between TCs and ENSO in the WNP is present not only in the observational records but is also captured by dynamical models (e.g., Wu and Lau 1992; Murakami et al. 2011; Chen and Tam 2010; Kim et al. 2014; Li and Wang 2014; Vecchi et al. 2014; Krishnamurthy et al. 2016). Over the decades, models ranging in complexity from atmospheric general circulation models (AGCMs) to coupled general circulation models (CGCMs) have been widely used to simulate the ENSO–TC connections (Wu and Lau 1992; Camargo and Sobel 2005; Murakami and Wang 2010; Murakami et al. 2011; Bell et al. 2014; Wang et al. 2014). The TC-permitting High Resolution Atmospheric Model (HiRAM) has produced promising simulations of interannual variability of hurricanes by prescribing the observed sea surface temperature (SST) in the North Atlantic (e.g., Zhao et al. 2009, 2010; Chen and Lin 2011, 2013). CGCMs have also shown encouraging ability to simulate the ENSO–TC connections across the tropics (Kim et al. 2014; Vecchi et al. 2014; Wang et al. 2014; Krishnamurthy et al. 2016; Murakami et al. 2015). AGCMs have been used for about two decades to simulate the ENSO–TC association in the WNP and have greatly advanced our understanding of the interannual variation of TCs over that region (Wu and Lau 1992; Vitart and Anderson 2001; Camargo et al. 2005; Murakami et al. 2011; Li and Wang 2014; Shaevitz et al. 2014). The 50-km AGCM used by Zhao et al. (2009) has lower skill in simulating the interannual variability of TC genesis frequency over the WNP than over the North Atlantic forced with SST prescribed from the observations. The value of AGCMs forced by historical SSTs to disentangle the role of climate variability on tropical cyclone activity is limited by relatively short integration lengths of these runs, as well as because the observed history of SSTs includes both the impact of radiative forcing and internal variability. In addition, AGCMs do not allow for ocean response to the atmosphere. Therefore, it is relatively difficult to isolate the impacts of such forcing when analyzing ENSO–TC connections. In contrast to a number of studies using AGCMs, relatively few studies have focused on the ENSO–TC association in the WNP by using CGCMs (Iizuka and Matsuura 2008; Bell et al. 2014; Kim et al. 2014; Vecchi et al. 2014; Krishnamurthy et al. 2016; Murakami et al. 2015).

High-resolution CGCMs have shown better skill than lower-resolution CCGMs in the simulation of ENSO variability (Shaffrey et al. 2009; Delworth et al. 2012; Dawson et al. 2013; Vecchi et al. 2014; Krishnamurthy et al. 2016; Murakami et al. 2015). A new high-resolution coupled climate model has been developed at the National Oceanic and Atmospheric Administration (NOAA)/Geophysical Fluid Dynamics Laboratory (GFDL), which is called the GFDL Forecast-Oriented Low Ocean Resolution version of CM2.5 (FLOR; Vecchi et al. 2014; Jia et al. 2015; Krishnamurthy et al. 2016; Yang et al. 2015a). FLOR was developed to be part of the North American Multimodel Ensemble (NMME; Kirtman et al. 2014). FLOR has been used to understand regional seasonal TC activity and to simulate and predict regional and extreme climate over regions of the world (Vecchi et al. 2014; Msadek et al. 2014; Jia et al. 2015, 2015, manuscript submitted to *J. Climate*) Krishnamurthy et al. 2015, 2016; Yang et al. 2015a,b; Zhang et al. 2016). Although FLOR produces a relatively satisfactory ENSO–TC association in the WNP, the responses of TC density and genesis to ENSO still have relatively large bias in this model (Vecchi et al. 2014; Krishnamurthy et al. 2016). The regions with positive correlation between Niño-3.4 and TC track density in the Pacific shift eastward to the eastern Pacific in FLOR and this shift in TC density may arise from stronger El Niño events in FLOR, with a more eastward extension to their convective anomalies resulting in an

enhanced negative response in the eastern Pacific and North Atlantic and the eastward extension of the western Pacific positive correlation (Vecchi et al. 2014; Krishnamurthy et al. 2016; Murakami et al. 2015). Recently, a new High-Resolution FLOR (HiFLOR) with 25-km mesh has been developed in GFDL. Initial results indicate that it produces much improved hurricane simulations, especially for category-4 and category-5 hurricanes (Murakami et al. 2015). The biases in the ENSO amplitude are also reduced in HiFLOR (Murakami et al. 2015). Based on these results, we assess whether and to what extent ENSO–TC connections in the WNP are better captured by HiFLOR. If HiFLOR indeed produces a better simulation of the ENSO–TC connections then this leads us to the question of how this impacts seasonal forecasting of TC activity and it provides us with an opportunity to advance our understanding of the mechanisms underpinning the ENSO–TC linkage from a modeling perspective. Better understanding of ENSO–TC interactions can in turn benefit the simulation and prediction of TCs in the WNP and produce more reliable projection of TC frequency, genesis, track, and landfall under global warming.

The remainder of this paper is organized as follows. Section 2 presents data and methodology and section 3 discusses the analysis results based on observation and simulations with FLOR and HiFLOR. Section 4 presents a discussion and conclusions.

2. Data and methodology

a. Data

This study uses the National Centers for Environmental Prediction (NCEP)–National Center for Atmospheric Research (NCAR) reanalysis (Kalnay et al. 1996) available from 1948, and the Japanese 55-year Reanalysis Project (JRA-55; Kobayashi et al. 2015) dataset from the Japan Meteorology Agency starting from 1961 for observed environmental large-scale circulation. Because the results based on two reanalysis datasets are consistent, we only show results from JRA-55. SST data are obtained from the Met Office Hadley Centre with a spatial resolution of 1° × 1° (Rayner et al. 2003). TC data are from the International Best Track Archive for Climate Stewardship (IBTrACS, v03r06; Knapp et al. 2010) released by the National Climatic Data Center (NCDC), including latitude, longitude, date, and intensity of historical TCs. The monthly precipitation data at 2.5° × 2.5° resolution are obtained from the National Aeronautics and Space Administration (NASA) Global Precipitation Climatology Project (GPCP), version 2.2, from 1979 to the present (Adler et al. 2003).

b. Climate models

Models used in this study include the state-of-the-art CGCMs FLOR and HiFLOR. The high-resolution TC-resolving coupled GFDL climate model FLOR was developed to study extreme weather and climate events such as TCs, extratropical cyclones, precipitation extremes, and floods (e.g., Vecchi et al. 2014; Jia et al. 2015, 2015, manuscript submitted to *J. Climate*; Yang et al. 2015a,b). The atmosphere and land components are identical to those of the GFDL Climate Model, version 2.5 (CM2.5; Delworth et al. 2012), with a spatial resolution of 50 km × 50 km. The ocean and sea ice components of FLOR are directly obtained from the CM2.1 with a spatial resolution of 1° × 1° except that there is refinement of the grid in the deep tropics (from 10°S to 10°N) to approximately 1/3° in the meridional direction. The relatively low-resolution ocean and sea ice components in FLOR are designed for a better efficiency of seasonal forecasting with large ensembles.

GFDL has developed a higher-resolution version of FLOR (HiFLOR) with a spatial resolution of 25 km based on FLOR (Murakami et al. 2015). HiFLOR was developed by increasing the horizontal resolution of atmosphere and land components while retaining the parameterized physical processes, with the ocean components directly inherited from FLOR except for the length of dynamical integration time steps in the atmosphere. Because of the increasing of the dynamical core atmospheric resolution, the dynamical time step in HiFLOR is half of that in FLOR. The "physics time step" (time step of the convection, cloud, and radiation schemes) in HiFLOR is kept the same as FLOR (Murakami et al. 2015). Therefore, the differences between FLOR and HiFLOR lie fundamentally in the horizontal spatial resolution of the atmosphere and land components.

c. Experiments

Control experiments were run for 300 years in HiFLOR and 1500 years in FLOR by prescribing radiative forcing representative of 1990. We selected the first 300 years from FLOR control experiment to be consistent with HiFLOR and to be compared with 300-yr control simulation of HiFLOR. Such experiments are "free run," in which flux adjustments (Magnusson et al. 2013; Vecchi et al. 2014) are not applied. It is noted that the control experiments are performed under idealized time-invariant forcing.

In addition to the control experiments with FLOR and HiFLOR, restoring experiments over the period 1971–2012 were performed with sea surface salinity (SSS) and SST restored to observational estimates of climatological SSS and interannually varying monthly SST at time scales of 5 and 10 days (Murakami et al. 2015). The simulated SSS in both models was restored to the *World Ocean Atlas 2005* (Antonov et al. 2006) values

TABLE 1. Classification of El Niño and La Niña years for the period of 1961–2013 based on the Niño-3.4 index.

El Niño	La Niña
1963, 1965,1969, 1972, 1976, 1982, 1987, and 1997	1964, 1970, 1973,1975, 1988, 1999, 2007, and 2010

TABLE 2. The standard deviation of Niño-3.4 index in the first 300 years of the control experiments with HiFLOR, FLOR, and observations (53 yr).

Magnitude	HiFLOR	FLOR	Observations
Niño-3.4	0.78	1.31	0.79

and SST was nudged (restored) to the monthly average field obtained from the Met Office Hadley Centre SST data (HadISST1.1; Rayner et al. 2003). The restoring experiments were conducted with three different initial conditions for both 5- and 10-day restoring time scales. The difference in TC simulation between 5- and 10-day restoring time scales was small for both FLOR and HiFLOR (Murakami et al. 2015), so we treat all six members as a single population from each model, thereby yielding six ensemble simulations each for FLOR and HiFLOR. Because both restoring experiments have the same prescribed SST and SSS, these experiments enable the diagnosis of whether and to what extent the differences in the ENSO–TC association between FLOR and HiFLOR arise from the improved performance of the SST simulation.

d. Classification of El Niño and La Niña years

The observed TC responses to ENSO are here used as a benchmark for the comparisons between FLOR and HiFLOR. The El Niño and La Niña years are defined based on the Niño-3.4 index, which is the SST anomalies averaged over the region 5°S–5°N, 170°E–120°W. The SST anomalies are defined as the deviation from the monthly climatology over the 1979–2000 period. The July–October (JASO) months during which the Niño-3.4 index is larger (smaller) than one standard deviation are designated as El Niño (La Niña) (Kim et al. 2009; Chen and Tam 2010). The La Niña and El Niño years for the period of 1961–2013 are listed in Table 1.

The strength of El Niño and La Niña events from the control experiments of FLOR and HiFLOR has a larger magnitude than the observations (Table 2). One standard deviation of the anomalous monthly SST is also used as the criterion for identifying El Niño or La Niña years for the FLOR and HiFLOR control experiments, which is consistent with Murakami et al. (2015). In the restoring experiments of FLOR and HiFLOR, we use the same definition of El Niño and La Niña years for the period 1971–2012 as in observations because SST was restored to observations. The central Pacific (CP) El Niño is not considered because there are few CP El Niño events in the control experiments of FLOR and HiFLOR. Krishnamurthy et al. (2016) found that the ENSO amplitude affects the ENSO–TC connections; therefore, if we select El Niño or La Niña years from the control experiments of FLOR and HiFLOR using the magnitudes of SST anomalies changing from 0.6° to 1.4°C at an interval of 0.1°C, the TC responses to ENSO are still consistent with those using one standard deviation of Niño-3.4. In general, the strength of responses of WNP TC to ENSO is indeed stronger for stronger ENSO events.

e. Landfall regions

Following previous studies (Wu et al. 2004; Zhang et al. 2012), the East Asian coast is divided into four subregions: Japan and the Korea Peninsula, the Philippines, Indochina and Malay Peninsula (ICMP), and China. The landfall frequencies are calculated for these four subregions, as well as for East Asia as a whole. Although the Philippines are geographically not part of East Asia, we consider them as one of the subregions since the Philippines are often severely threatened by landfalling tropical systems (Wu et al. 2004; Chan and Xu 2009; Zhang et al. 2012). In general, TCs are more likely to make landfall over East Asia during La Niña than El Niño phases.

3. Results

This section discusses the analysis of TC activity (e.g., density, genesis, and landfall) during El Niño and La Niña phases and examines the ENSO–TC association and underlying mechanisms. This is accomplished based on the control experiments and SSS- and SST-restoring ensemble experiments with both FLOR and HiFLOR and observations.

a. Results from control experiments

TC density climatology in the 300-yr control experiments of HiFLOR, FLOR, and observations is shown in Fig. 1. TC track and genesis density is obtained by binning the TC tracks and geneses in the WNP in 5° × 5° grid boxes without smoothing. The detailed tracking processes are provided in the appendix. Although the spatial patterns of the TC density climatology in the control experiments of HiFLOR and FLOR are similar, the TC density climatology in HiFLOR is larger than that in FLOR (Fig. 1). In contrast to the observations, the centers of TC track density in HiFLOR and FLOR

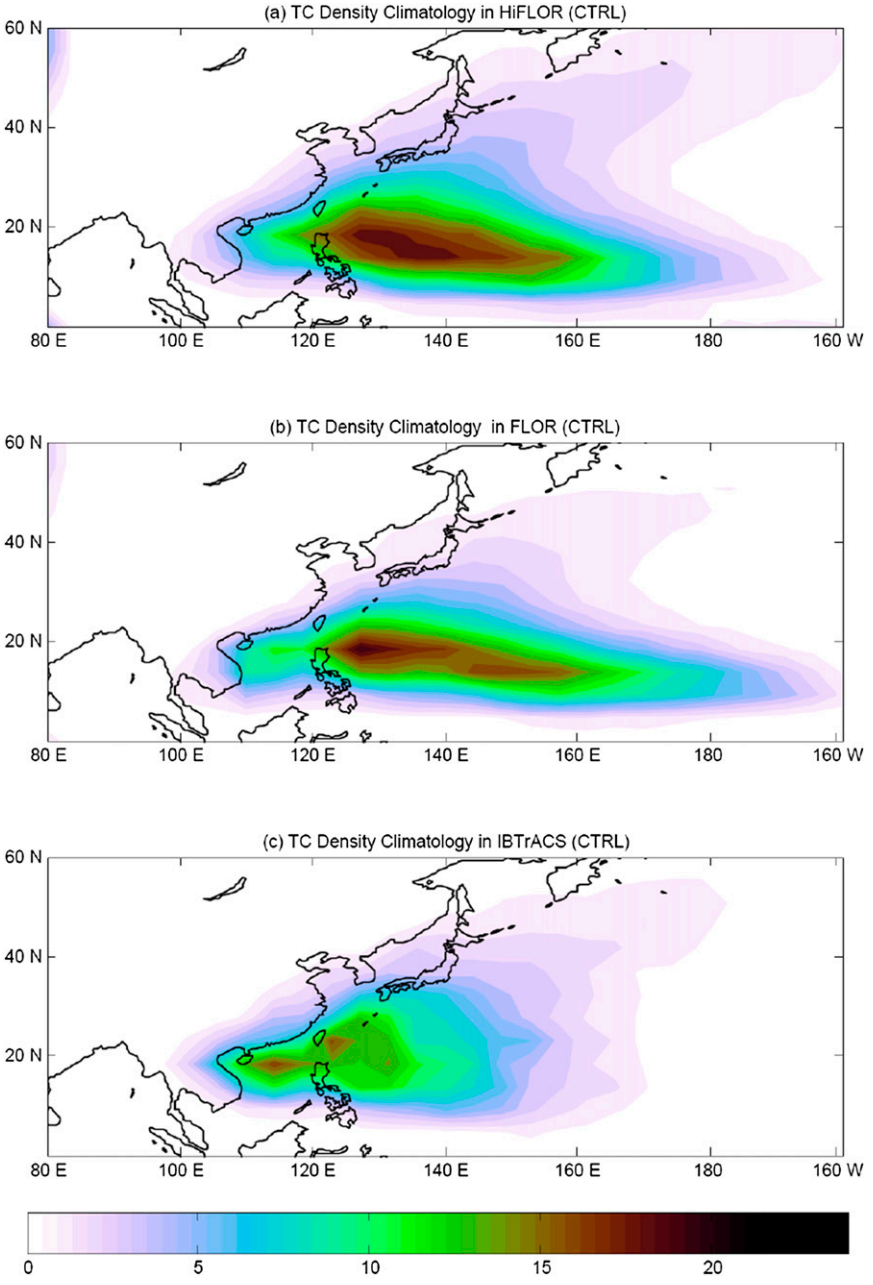

FIG. 1. TC density climatology (No. of times per year) in the control experiments (300 yr) of (a) HiFLOR and (b) FLOR and (c) observations (1961–2013).

are located eastward (Fig. 1) and such spatial characteristics have also been reported in previous studies (Vecchi et al. 2014; Murakami et al. 2015). Similar to the TC track density climatology, the climatology of TC genesis density in the control experiments of HiFLOR and FLOR is located eastward of that in observations (Fig. 2). However, the TC genesis density pattern in HiFLOR is closer than that in FLOR to the observations, especially from 120° to 150°E (Fig. 2). The differences in TC genesis and density climatology between HiFLOR and FLOR (HiFLOR minus FLOR) are characterized by a dipole pattern in the WNP (i.e., positive anomalies in the eastern part of the WNP and negative anomalies in the western part of the WNP; Fig. S1 in the supplemental material). The seasonal cycle of WNP TC frequency in HiFLOR, FLOR, and observations is consistent with the above discussion on TC genesis (Fig. S2 in the supplemental material). HiFLOR

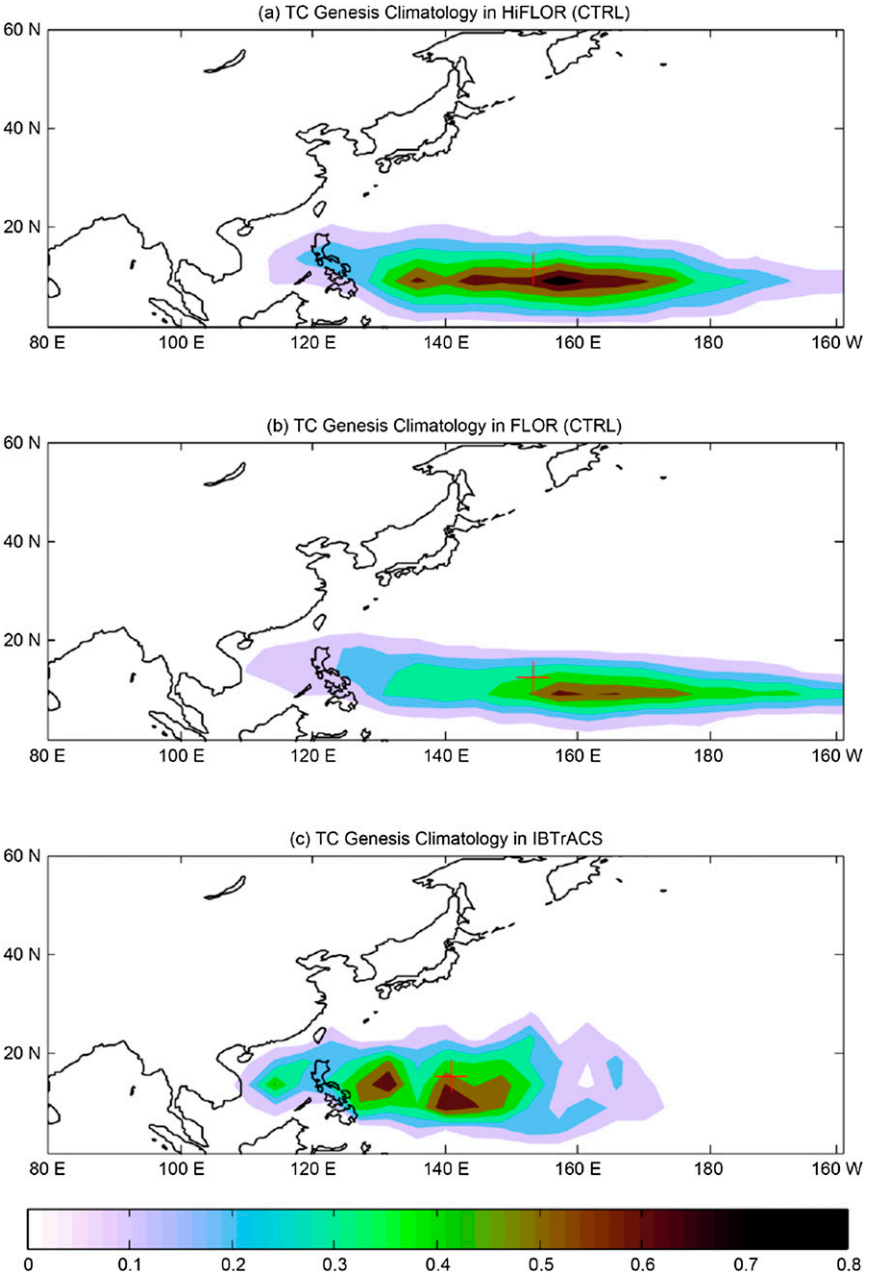

FIG. 2. TC genesis climatology (No. of times per year) in the control experiments (300 yr) of (a) HiFLOR, (b) FLOR, and (c) observations (1961–2013). The red plus sign represents the mean TC genesis location.

simulates TCs more than observations in the WNP for each month and more than FLOR from April to September (Fig. S2), similar to what is presented by Murakami et al. (2015). However, HiFLOR produces a more faithful representation of the phasing of seasonal cycle of TC frequency in the WNP than FLOR, with the peak in FLOR occurring a month or so after the August peak observed and in HiFLOR (Fig. S2). The improvements in the seasonal variation of TC frequency are consistent with previous studies reporting that an increase in horizontal resolution of a climate model results in better seasonal variation of TC frequency in a coupled climate model (Murakami and Sugi 2010). The simulated mean frequency of TC landfall over East Asia and its subregions in the control experiment of HiFLOR is better than that in FLOR (Fig. S3 in the supplemental

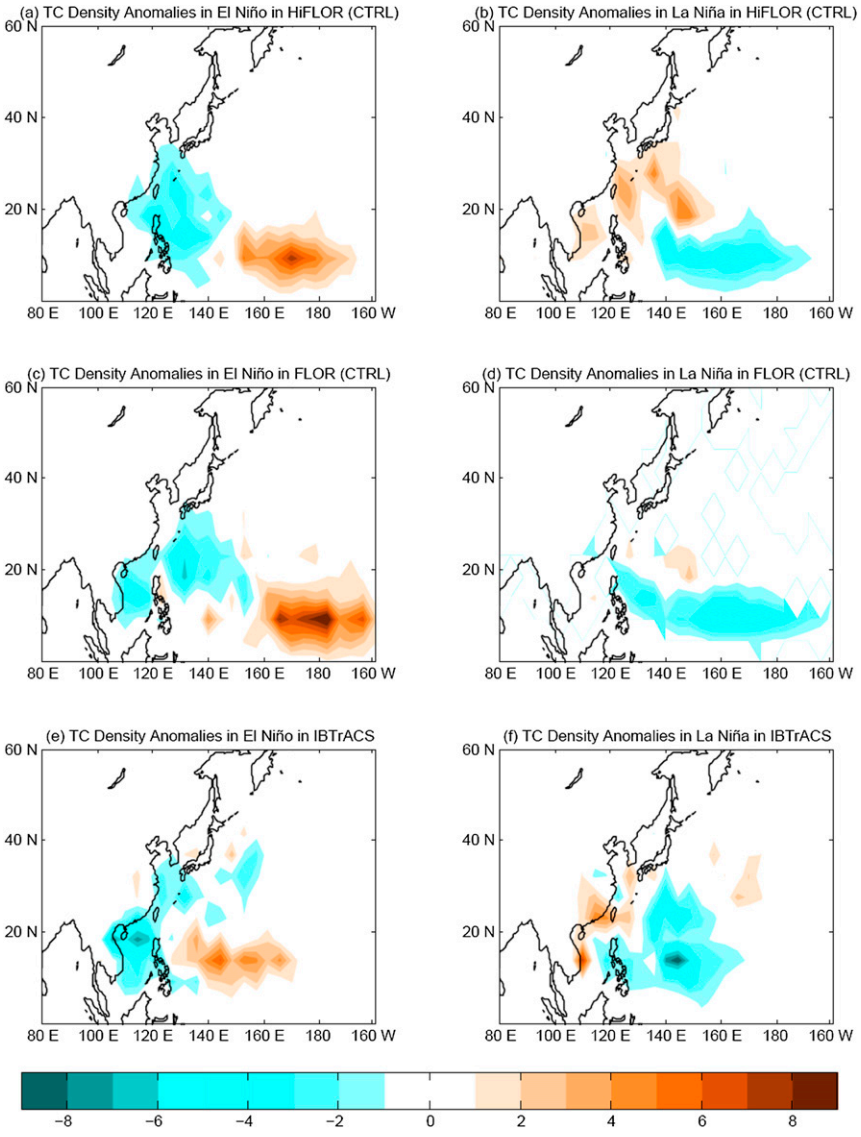

FIG. 3. TC track density anomalies (No. of times per year; binned into 5° × 5° grid box) in the WNP during El Niño and La Niña phases based on (a),(b) HiFLOR, (c),(d) FLOR, and (e),(f) observations.

material). A better simulation of TC climatology can play some role in improving the simulated responses of TCs to ENSO.

Distinct differences in TC track density anomalies are found between El Niño and La Niña conditions in the 300-yr control experiments with HiFLOR (Figs. 3a,b). During the El Niño phase of HiFLOR control simulation, positive (negative) TC density anomalies are identified in the eastern (western) WNP. During the La Niña phase, the spatial pattern of TC density anomalies is largely the opposite of what discussed for the El Niño phase although positive anomalies are relatively weak in the Philippine Sea and the South China Sea (Figs. 3a,b). In the El Niño phase of FLOR control simulation, the positive TC density anomalies are stronger and shifted more eastward toward the central Pacific than HiFLOR. In the La Niña phase of the control simulations with FLOR, the negative TC density anomalies shift more eastward and prevail in the entire WNP. Such TC density patterns during the ENSO phases with FLOR or CM2.5 have been identified in previous studies (Kim et al. 2014; Vecchi et al. 2014; Krishnamurthy et al. 2016; Murakami et al. 2015).

TC density anomalies in HiFLOR are more consistent with observations than FLOR during both El Niño and La Niña phases. In the El Niño phase, the centers of

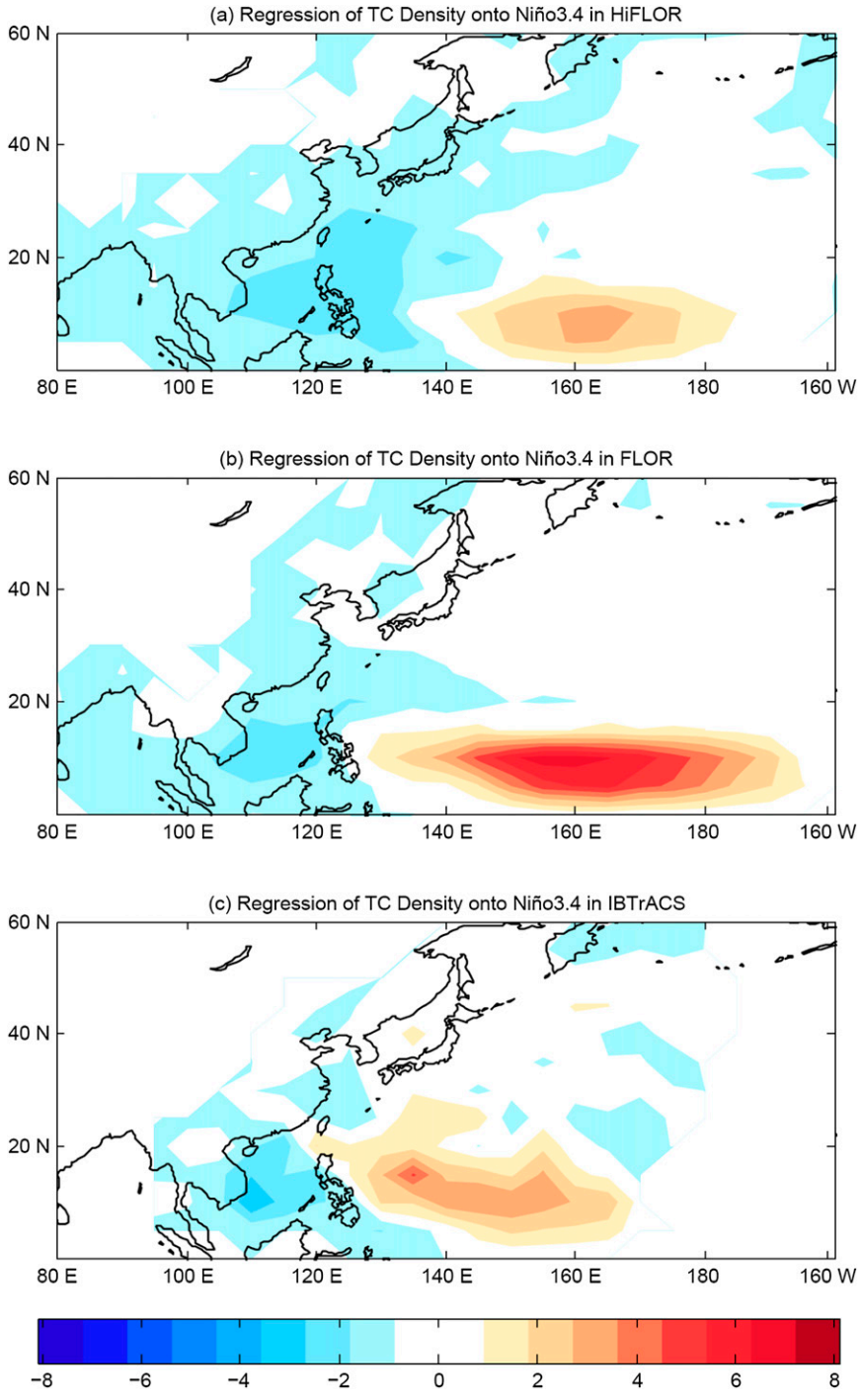

FIG. 4. Regressions of TC track density (No. of times per year; binned into 5° × 5° grid box) onto Niño-3.4 based on the control experiments with (a) HiFLOR and (b) FLOR and (c) observations.

positive TC density anomalies are shifted more westward in HiFLOR than in FLOR (Fig. 3) with the spatial pattern of negative or positive TC density anomalies in HiFLOR closer to the observations, although some eastward bias still exists. During El Niño, there are positive TC density anomalies around the Philippines in FLOR while there are negative TC density anomalies in HiFLOR and the observations in this region. In the La

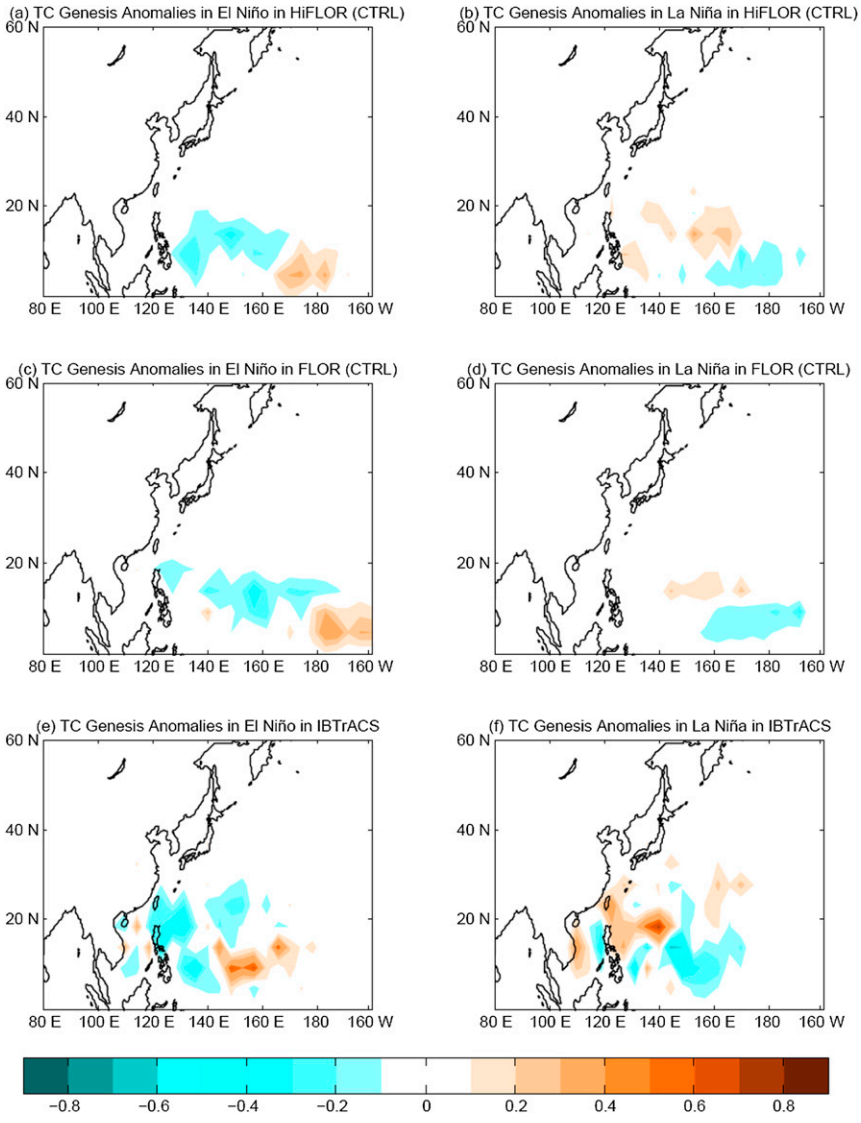

FIG. 5. TC genesis anomalies (No. of times per year; binned into 5° × 5° grid box) in the WNP during El Niño and La Niña phases based on the control experiments with (a),(b) HiFLOR and (c),(d) FLOR and (e),(f) observations.

Niña phase, HiFLOR produces a better simulation of TC track density than FLOR, in that both HiFLOR and observations show positive TC density anomalies in the South China Sea and the East Asian coast in contrast to basinwide negative TC density anomalies in FLOR.

The regressions of TC density onto Niño-3.4 are shown to further substantiate the previous discussion (Fig. 4). The regressions of TC track density anomalies onto the Niño-3.4 index with HiFLOR resemble those from observations while the positive anomalies from FLOR have a much higher magnitude (Fig. 4). This indicates that the responses of TC density to ENSO in FLOR are much stronger than the observations and HiFLOR. Although the positive anomalies of TC track density in HiFLOR control experiments are shifted slightly eastward when compared to the observations (although less so than in FLOR), the magnitude of anomalous TC track density is in good agreement (Fig. 4). Compared with the observations, regression analysis discussed above suggests that the responses of TC density to a unit of Niño-3.4 (i.e., 1°C) are stronger in FLOR than either HiFLOR or observations, especially in the eastern part of the WNP. Different sample sizes (time period) in the control experiments and observations may bias the above results. We calculate the regression of TC track density onto Niño-3.4 index in each

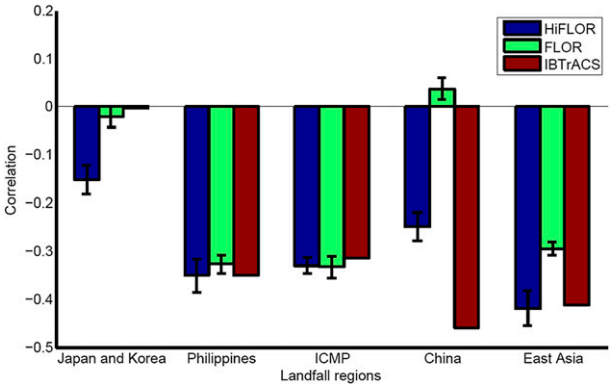

FIG. 6. Correlation between Niño-3.4 and TC landfall frequency over Japan and the Korea Peninsula, the Philippines, ICMP, China, and East Asia in the 300-yr control experiments of FLOR and HiFLOR and in the observations. The correlation for HiFLOR and FLOR are calculated by averaging the correlation coefficients for every 53-yr moving periods and the error bars represent the confidence interval of the average correlation coefficients for each 53-yr period at a 0.05 level of significance. The observations cover the period 1961–2013.

53-yr subperiod [the same as the time period (1961–2013) of observations] in the control experiments of HiFLOR and FLOR (not shown). It appears that the regression of TC density onto Niño-3.4 over the entire 300 years is consistent with those over every 53-yr subperiod in the control experiments of HiFLOR and FLOR.

Consistent with the above discussion, HiFLOR also produces TC genesis anomalies that are in closer agreement with the observations than FLOR in ENSO phases (Fig. 5). Specifically, TC genesis anomalies in FLOR are located substantially farther eastward than in the observations during the El Niño phase. In contrast, TC genesis in HiFLOR is located more westward than in FLOR, more similar to observations in the El Niño phase (Fig. 5). During the La Niña phase, FLOR does not reproduce the observed positive anomalies west of 140°E, whereas HiFLOR shows the positive TC genesis anomalies, especially over the area from 120° to 140°E (Fig. 5).

Previous studies have reported that landfalling TCs over East Asia are more likely to occur in La Niña years than El Niño years because of a westward shift in the subtropical high during la Niña years which subsequently produces an increase in TC landfall in the WNP (Wang and Chan 2002; Wu et al. 2004; Zhang et al. 2012). Figure 6 shows the correlation coefficients between the frequency of TCs making landfall over East Asia and four subregions and Niño-3.4 in the control simulation of FLOR and HiFLOR and observations (1961–2013). The correlation in HiFLOR more closely resembles what obtained from the observation than in FLOR except for TC landfall over Japan and the Korea Peninsula (Fig. 6). There is a much stronger positive correlation between landfall over Japan and the Korea Peninsula during La Niña in HiFLOR than observations (Fig. 6). In addition, the correlation between TC landfall over China and Niño-3.4 in FLOR is positive while it is negative in the observations and HiFLOR (Fig. 6). HiFLOR therefore makes a substantial improvement in simulating the responses of TC landfall over China to ENSO. It is of great significance because China is a heavily populated country and has the longest coastline in East Asia. Moreover, the association between the frequency of TC landfall over East Asia and subregions and Niño-3.4 is largely better simulated in HiFLOR than in FLOR. The improved connection between TC track density and ENSO in HiFLOR is thus reflected in a better connection between TC landfall and ENSO.

b. Mechanisms from control experiments

ENSO alters remote large-scale circulation by teleconnections (Lau and Nath 1996; Alexander et al. 2002). The modulation of the Walker circulation by ENSO strongly shapes the ENSO–TC connections in the WNP in FLOR and HiFLOR. The SST, precipitation, Walker circulation, and steering flow during El Niño and La Niña phases in HiFLOR, FLOR, and observations are discussed to identify the underlying mechanisms.

The standard deviation of Niño-3.4 in HiFLOR is smaller than those in FLOR but still larger than in the observations (Table 2). The SST anomaly patterns during El Niño and La Niña phases from HiFLOR, FLOR, and the observations are shown in Fig. 7; SST anomalies in FLOR are stronger than those in HiFLOR and in the observations for both El Niño and La Niña phases, especially in the ENSO regions (Figs. 7a,c,e). A larger magnitude of Niño-3.4 in FLOR may be responsible for the stronger responses of TC density to ENSO as shown in Fig. 2 (Krishnamurthy et al. 2016; Murakami et al. 2015).

Precipitation is closely linked to SST anomaly patterns. Precipitation is associated with deep convection in the atmosphere, which alters local and remote circulation (Trenberth et al. 2002; Chiang and Lintner 2005). During El Niño years, the FLOR precipitation anomalies are stronger than those in HiFLOR and in the observations in the tropical central Pacific, indicating that the responses of precipitation to SST anomalies in HiFLOR bear more resemblance than FLOR to those in the observations (Fig. 8). During La Niña years, the major differences in precipitation anomalies between HiFLOR and FLOR are located in the southeastern WNP (depicted by the rectangles in Figs. 8d and 8f). The

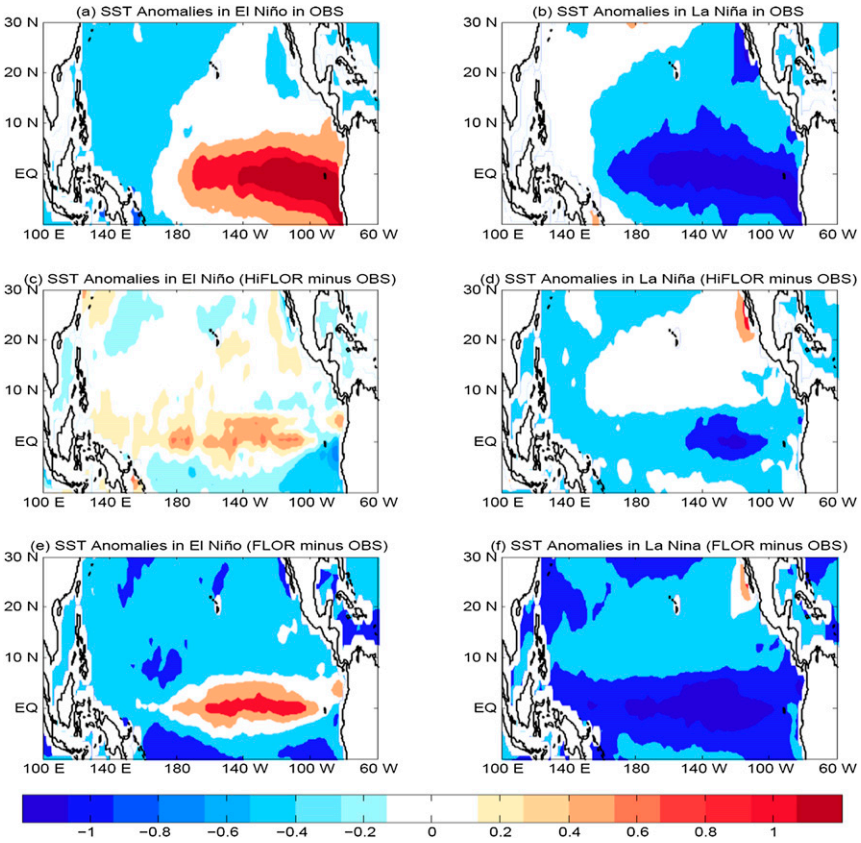

FIG. 7. SST anomalies (°C) during El Niño and La Niña phases based on control experiments with (a),(b) observations, (c),(d) HiFLOR − observations, and (e),(f) FLOR − observations.

precipitation anomalies in the marked regions of Fig. 8 are also reflected in the Walker circulation (Fig. 9).

TC activity in the WNP is largely modulated by dynamic factors associated with changes in large-scale circulation rather than local thermodynamic changes connected to local SST (Chan 2000; Wang and Chan 2002; Chan and Liu 2004; Fu et al. 2012). Changes in the Walker circulation are exhibited in the vertical profiles of zonal wind (averaged over 5°–20°N) and vertical pressure velocity (ω) scaled by $-50\,\mathrm{Pa\,s^{-1}}$ (Fig. 9). During El Niño years, the anomalous updraft in the tropical central Pacific in FLOR is much stronger than those in HiFLOR and observations (i.e., JRA-55 reanalysis) (Fig. 9), suggesting stronger deep convection over that region in FLOR. Such results corroborate the analysis of TC density and genesis anomalies in HiFLOR, FLOR, and the observations (Figs. 3 and 4).

During La Niña years, the updraft anomalies in the control simulation of FLOR are still greater than in HiFLOR and the anomalous downdraft in FLOR is also stronger than in HiFLOR in the WNP (Fig. 9), resulting in strong suppression of WNP TC activity in FLOR. In addition, the Walker circulation in HiFLOR is more realistic than that in FLOR, particularly the anomalous ascent in the WNP and the anomalous subsidence in the tropical eastern and central Pacific (Fig. 9d). The excessive anomalous Walker circulation appears to be responsible for the heightened negative TC density and genesis anomalies in the WNP during La Niña years in the FLOR control experiment.

Figure 10 illustrates the differences in the steering flow (850–200-hPa mass-weighted mean) between HiFLOR and FLOR in the control experiments during El Niño and La Niña phases. HiFLOR produces a stronger easterly steering flow than FLOR in both El Niño and La Niña phases, indicating that WNP TCs are more likely to move westward in HiFLOR given the same genesis locations (Fig. 10). The effects of steering flow appear to be highly distinct in the La Niña phase in the control experiments of HiFLOR and FLOR because TC density in HiFLOR is much higher than that in FLOR (Figs. 3 and 9). Although higher TC genesis in the Philippine Sea may play some role in shaping the differences in TC density between HiFLOR and FLOR, the steering flow should act as a key factor to produce different TC density patterns during La Niña phase.

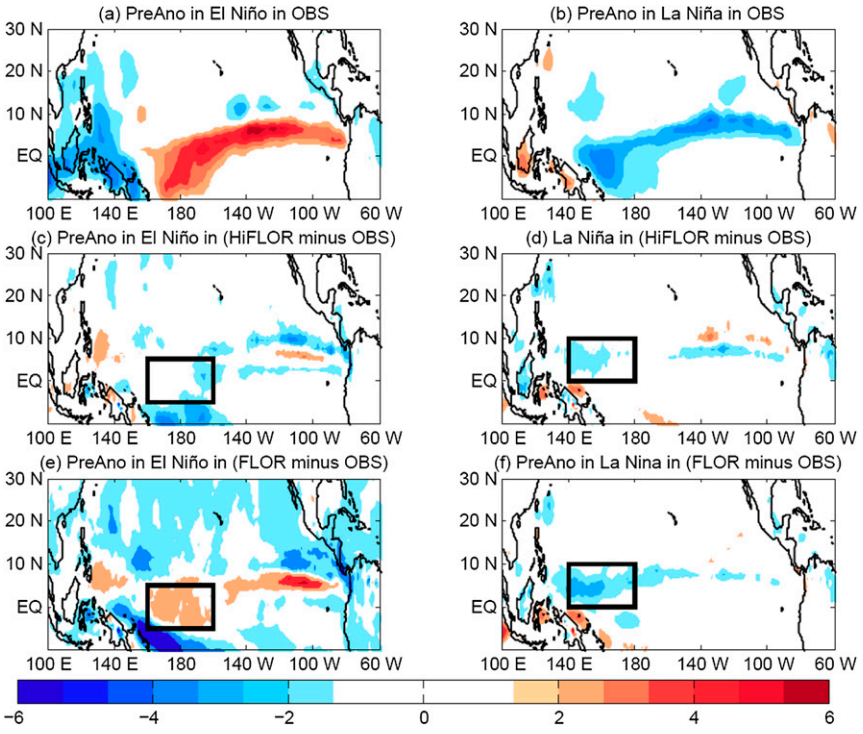

FIG. 8. Precipitation anomalies (PreAno; mm day^{-1}) during El Niño and La Niña phases based on (a),(b) observations, (c),(d) HiFLOR − observations, and (e),(f) FLOR − observations.

Previous studies have shown that the beta drift due to Coriolis force changes related to TC size also influence TC tracks (Wu and Wang 2000, 2001). As shown in Murakami et al. (2015), TC sizes in FLOR and HiFLOR are very close to one another, indicating that beta drift is not an important factor in causing the differences between FLOR and HiFLOR.

c. *SST-restoring experiments*

The previous discussion has shown that the responses of TC density, genesis, and landfall to ENSO are greatly improved in HiFLOR than FLOR in the control experiments. Since the ENSO SST anomalies in FLOR are much stronger than those in HiFLOR and in the observations, it is useful to assess whether the ENSO–TC improvements are caused by a better representation of SST in HiFLOR. We do so by exploring whether, and the extent to which the improvements between HiFLOR and FLOR in simulated ENSO–TC relationship still hold in the additional SST and SSS restoring ensemble experiments which control for differences in SST simulation in the coupled models.

The climatology of TC track density in the SSS- and SST-nudging experiments of HiFLOR is larger than that in FLOR in period 1971–2012 and both have similar spatial patterns (Fig. 11). The high centers of TC track density climatology in HiFLOR and FLOR reside eastward of those in the observations in 1971–2012 (Fig. 11). The high centers of TC genesis density climatology in HiFLOR and FLOR are also located eastward of that in the observations (Fig. 12). However, the genesis density climatology in HiFLOR is located less eastward than that in FLOR, indicating a stronger resemblance to the observations than FLOR (Fig. 12). The seasonal variation of WNP TC frequency in HiFLOR more closely resembles the observations than FLOR, although there is a higher TC frequency in HiFLOR for each month (Fig. S3). The climatology of TC landfall frequency over the Philippines, ICMP, China, and East Asia in the SSS- and SST- restoring experiment of HiFLOR appears to be close to or better than those in FLOR, while FLOR outperforms HiFLOR for TC landfall over Japan and the Korea Peninsula (Fig. S4 in the supplemental material).

In the El Niño phase, TC track density anomalies in the SST-restoring experiments with HiFLOR are consistent with those in the observations, while those with FLOR differ considerably from observations (Fig. 13). Both TC track density anomalies in the SST-restoring experiments with HiFLOR and the observations

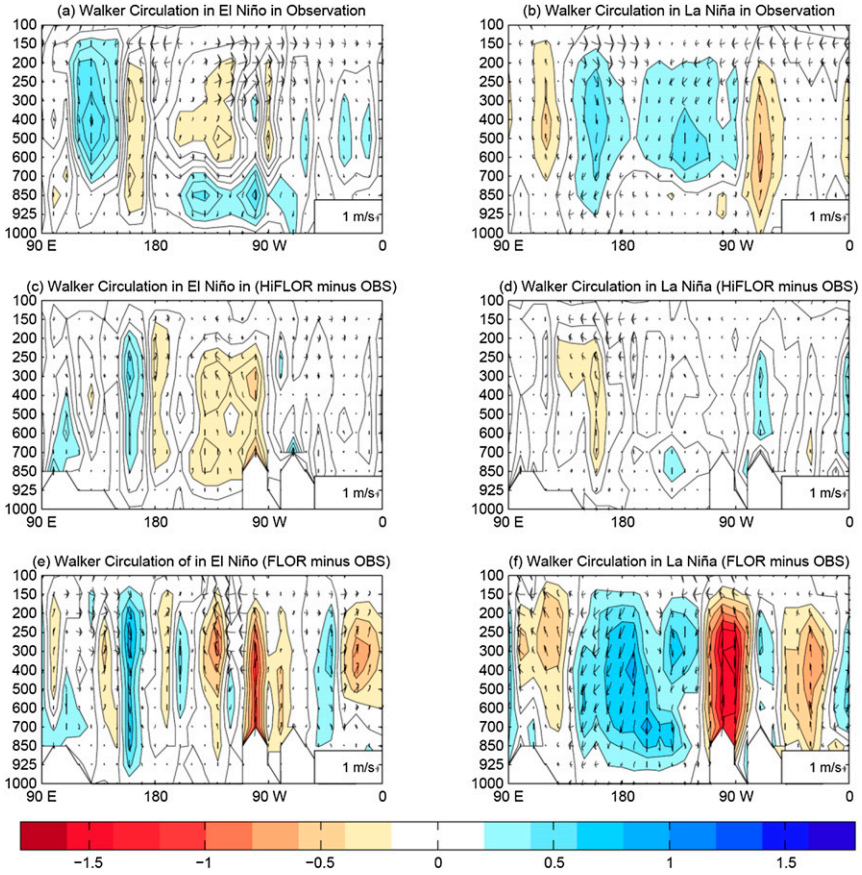

FIG. 9. Vertical profile in pressure (hPa) of wind vectors [zonal wind (averaged over 5°–20°N) and ω scaled by -50 Pa s^{-1}] during El Niño and La Niña phases based on (a),(b) observations, (c),(d) HiFLOR − observations, and (e),(f) FLOR − observations. The shading represents the unscaled ω.

feature a dipole mode in the WNP (Fig. 13). In contrast, the TC track density anomalies in the SST-restoring experiments with FLOR have strong positive anomalies in the eastern WNP (Fig. 13). During El Niño years, there are negative TC density anomalies near the East Asian coast in both observations and the SST-restoring experiments with HiFLOR, while negative anomalies are not observed in FLOR. Instead, positive TC density anomalies are observed in the northern Philippines (Fig. 13c). During La Niña years, positive TC track density anomalies prevail along the East Asian coast, while there are strong negative TC track density anomalies in the WNP in the observations (Fig. 13f). Such TC density anomalies suggest more TCs making landfall over East Asia during the La Niña phase (Wu et al. 2004; Zhang et al. 2012). The SST-restoring experiments with HiFLOR largely reproduce the TC track density anomalies in the observations during La Niña (Fig. 13b). The TC track density anomalies in FLOR (Fig. 13d), however, are quite different from those in the observations because there are negative TC density anomalies almost everywhere in the WNP. Based on the SST-restoring experiments with FLOR, there are fewer TC landfalls over East Asia during La Niña years, opposite to what is found in the observations. Therefore, our finding that HiFLOR produces better responses of TC to ENSO than FLOR based on 300-yr control experiments also holds for the SST-restoring ensemble experiments.

The differences in TC genesis locations between HiFLOR and FLOR are mainly located west of 150°E (Fig. 14). During the El Niño phase, negative TC genesis anomalies are stronger in FLOR than HiFLOR west of 150°E. TC density anomalies in FLOR, however, are higher than in HiFLOR in the vicinity of the East Asian coast during the El Niño phase. During the La Niña phase, positive TC genesis anomalies are stronger in HiFLOR than in FLOR west of 150°E, consistent with TC density patterns (Figs. 13 and 14). However, TC genesis cannot fully explain the spatial patterns of TC

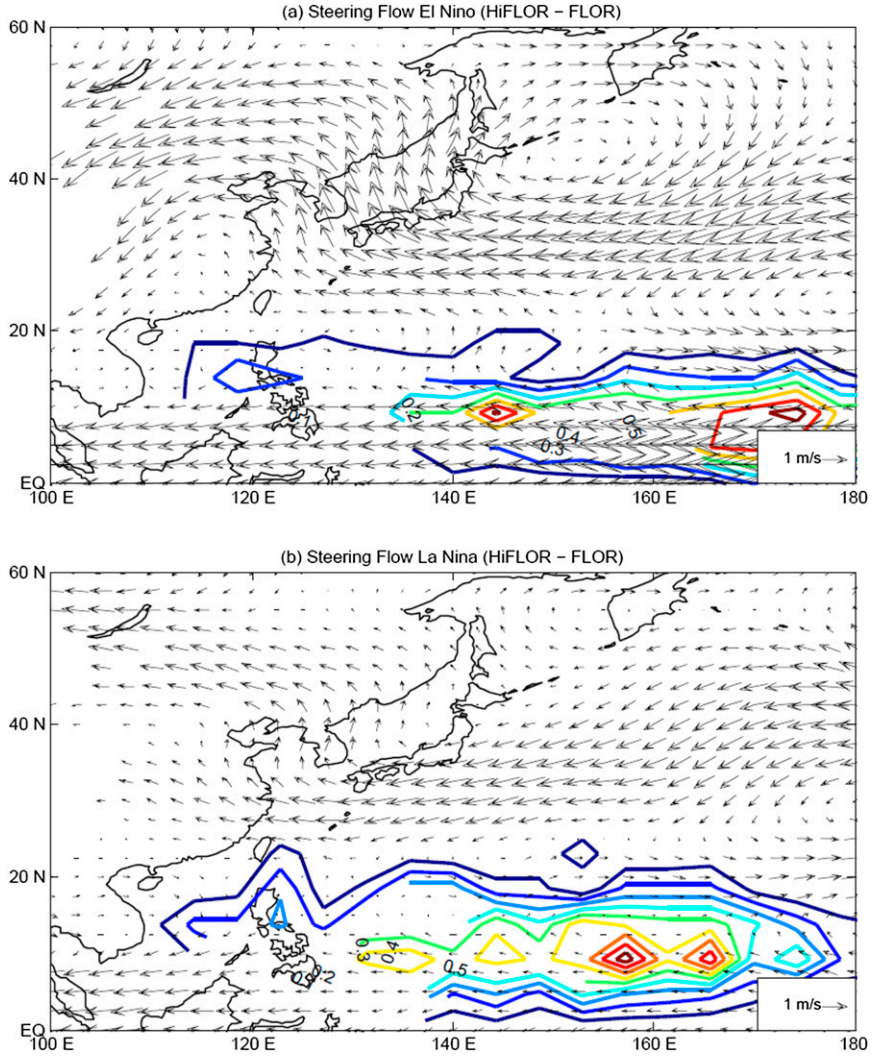

FIG. 10. Differences in steering flow (HiFLOR minus FLOR; $m\,s^{-1}$) in the control experiments during (a) El Niño and (b) La Niña years. Contours represent the annual average TC genesis density in the control experiment of HiFLOR.

density, especially during the El Niño phase. Therefore, the steering flow between HiFLOR and FLOR may be responsible for the differences in TC density.

The correlations between TC landfall and Niño-3.4 based on FLOR, HiFLOR, and observations are listed in Table 3. Such correlations are consistent with those in the control experiments (Fig. 6). HiFLOR reproduces the negative correlation between the frequencies of TCs making landfall over East Asia and the subregions and Niño-3.4 in the observational records, although the correlation coefficients have a larger magnitude (Table 3). In contrast, FLOR produces positive correlation coefficients between Niño-3.4 and the frequencies of TCs making landfall over China and East Asia, with the wrong sign compared with those based on observations (Table 3). Meanwhile, the correlation coefficients between Niño-3.4 and the frequencies of TCs making landfall over Japan and the Korea Peninsula, the Philippines, and ICMP in FLOR are similar to those in observations.

d. Mechanisms from SST-restoring experiments

Since SSTs in the restoring experiments with HiFLOR and FLOR are restored to the observations, only the precipitation, Walker circulation, and steering flow during El Niño and La Niña phases are discussed here.

During the El Niño phase, the precipitation anomalies located in the WNP in the HiFLOR and FLOR restoring experiments are largely weaker than those in the observations (Fig. 15). The precipitation anomalies in HiFLOR and FLOR are similar to one another in the

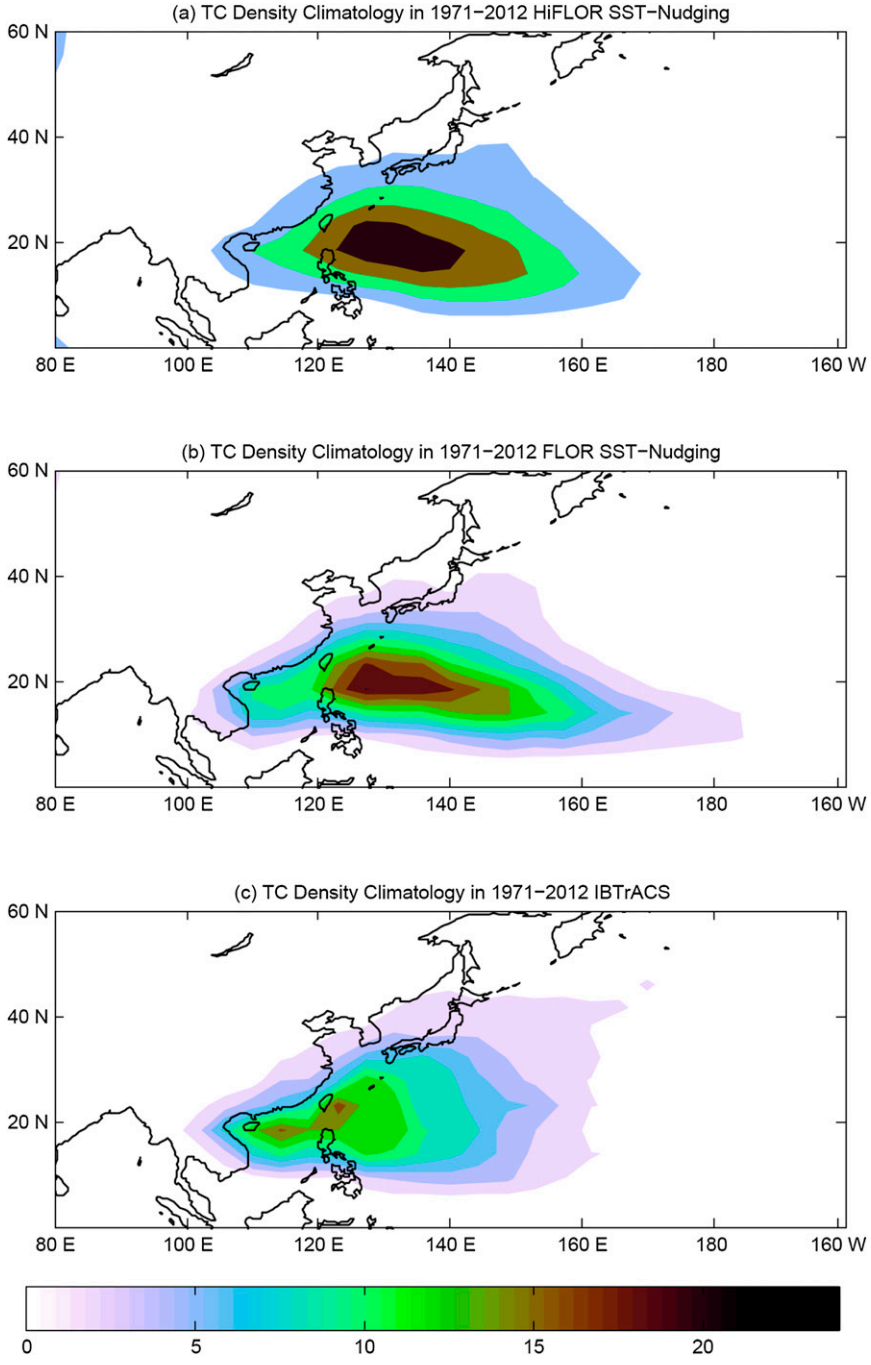

FIG. 11. The simulated TC density climatology (No. of times per year) in the SSS- and SST-nudging experiments of (a) HiFLOR and (b) FLOR and (c) observations (1971–2012).

WNP, suggesting similar strengthen of deep convection in HiFLOR and FLOR (Fig. 15). During the La Niña phase, the precipitation anomalies in the WNP in FLOR and HiFLOR are similar to the observations (Fig. 15).

This is in contrast with the precipitation anomalies in HiFLOR and FLOR for the control experiments, where FLOR produces stronger positive anomalies in precipitation than HiFLOR. The SST-restoring experiments of FLOR and HiFLOR have similar observationally based SST patterns, but FLOR overestimates ENSO amplitude in its control experiment. The weaker responses of precipitation to El Niño and La Niña in the

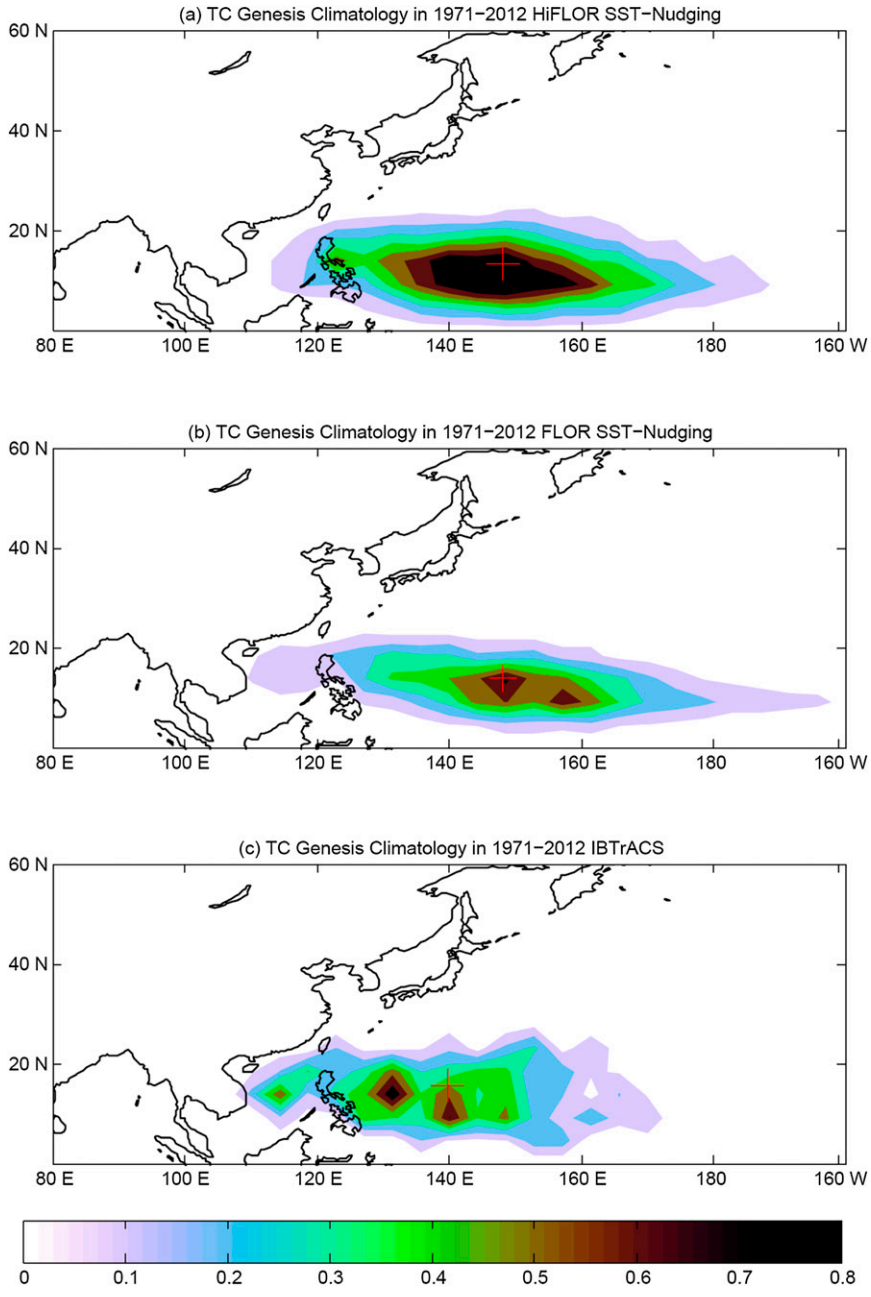

FIG. 12. The simulated TC genesis climatology (No. of times per year) in the SSS- and SST-nudging experiments of (a) HiFLOR and (b) FLOR and (c) observations (1971–2012). The red plus sign represents the mean TC genesis location.

restoring experiments of FLOR may arise from the weaker SST anomalies compared with the control experiments of FLOR. This also indicates the important role SST plays in shaping the deep convection.

Figure 16 shows the vertical profile of the wind vector, that is, zonal wind (averaged over 5°–20°N),and ω scaled by $-50\,\mathrm{Pa\,s^{-1}}$ during El Niño and La Niña phases based on the SST-restoring experiments with HiFLOR, FLOR, and the observations. The differences in the Walker circulation between FLOR and HiFLOR are mainly located within 110°–150°E (Fig. 16). In the El Niño phase, the updraft anomalies in FLOR are stronger than HiFLOR in 110°–150°E. In the La Niña phase, the downdraft anomalies in FLOR are also stronger than HiFLOR in 110°–150°E (Fig. 16). This is consistent with the differences in TC genesis anomalies between HiFLOR and

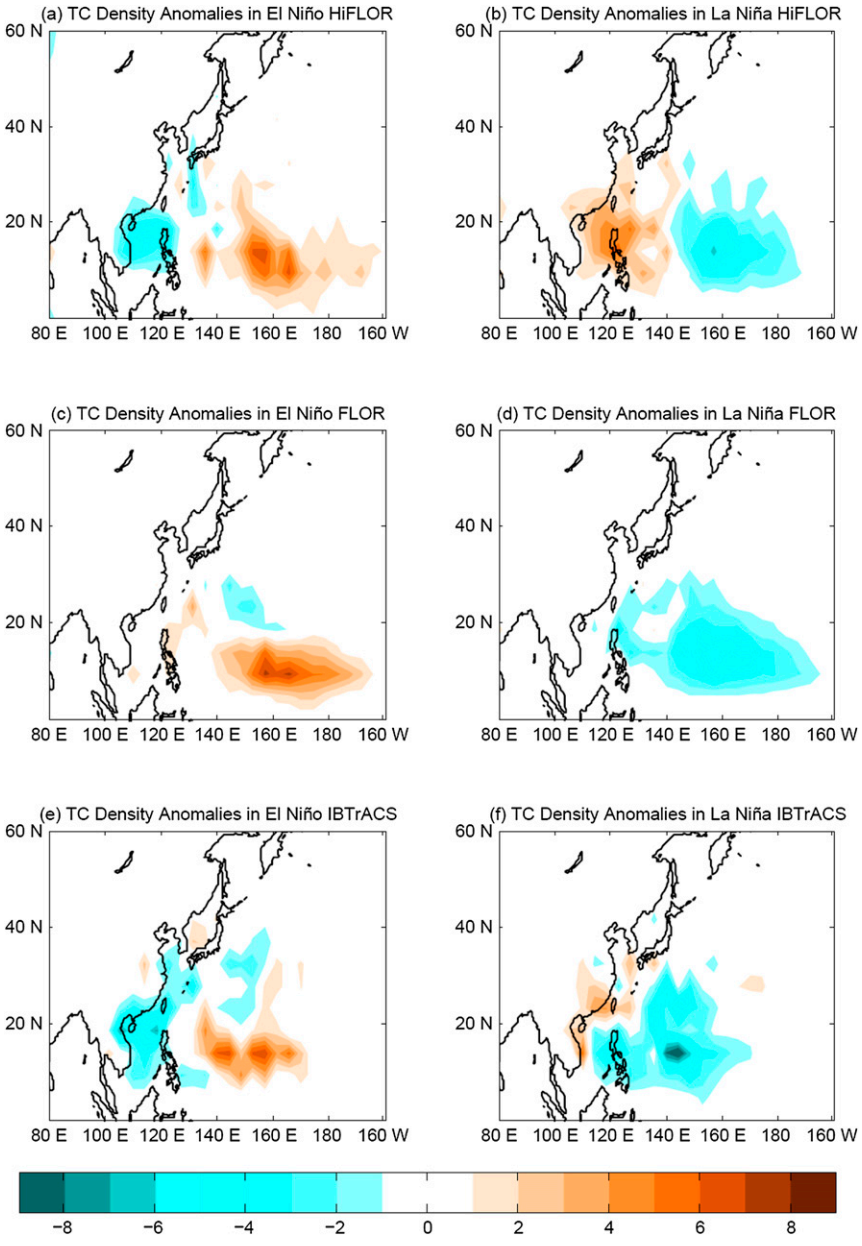

FIG. 13. TC track density anomalies (No. of times per year; binned into 5° × 5° grid box) in El Niño and La Niña events in the SST-restoring experiments of (a),(b) HiFLOR and (c),(d) FLOR and (e),(f) the observations.

FLOR during El Niño and La Niña years in 110°–150°E (Fig. 14)

Figure 13 also shows that TCs in FLOR tend to move toward the East Asian coast in the El Niño phase while they tend to stay in the ocean during the La Niña phase. In addition to the spatial patterns of TC genesis, the differences in steering flow between HiFLOR and FLOR (HiFLOR − FLOR) SST-nudging experiments are also analyzed during both El Niño and La Niña phases (Fig. 17). Steering flow (850–200 hPa) is more favorable for TCs to move eastward in HiFLOR than FLOR during the El Niño phase (Fig. 17). Meanwhile, steering flow is more conducive to westward-moving TC track from 10° to 20°N in HiFLOR than FLOR during the La Niña phase (Fig. 17). This is partly responsible for strong negative TC track density anomalies in the WNP in FLOR and strong positive TC track density anomalies along the East Asian coast in

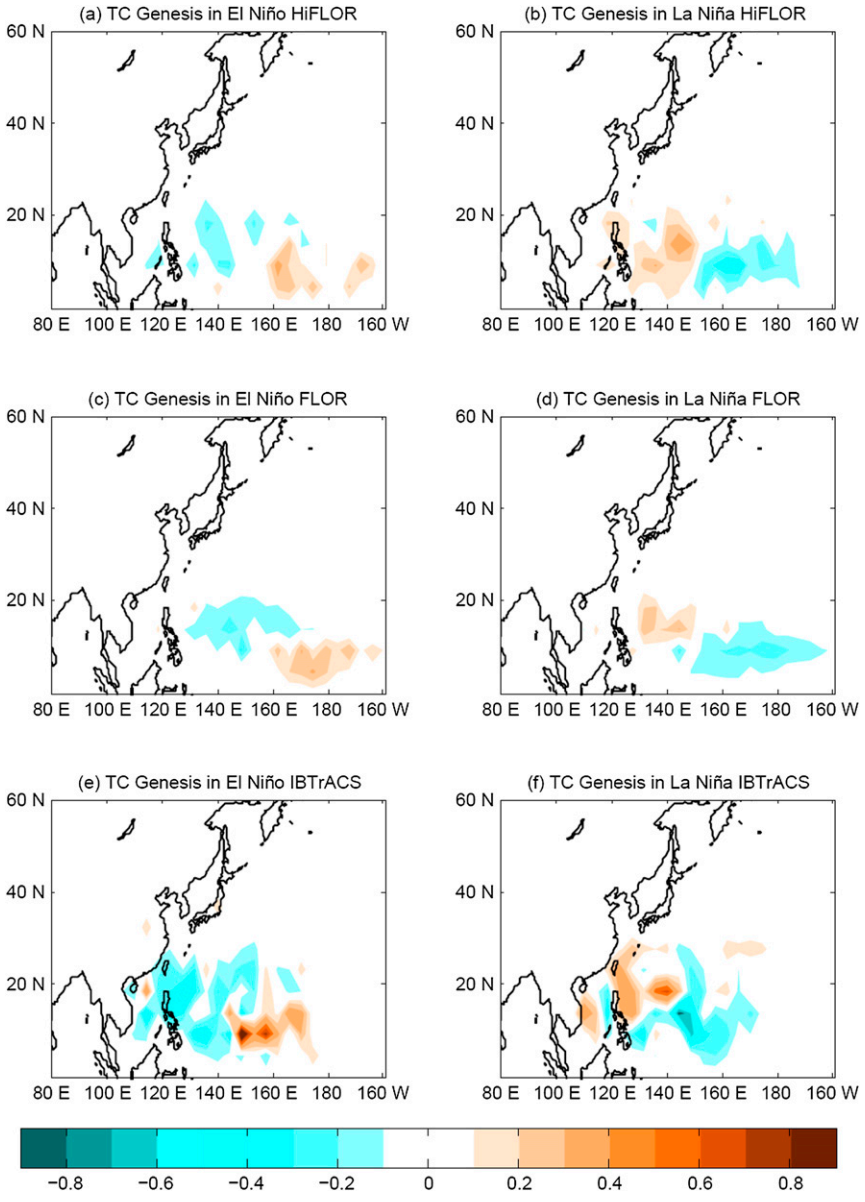

FIG. 14. Annual average TC genesis anomalies (No. of times per year; binned into 5° × 5° grid box) during El Niño and La Niña events in SST-restoring experiments with (a),(b) HiFLOR and (c),(d) FLOR and (e),(f) observations.

HiFLOR during the La Niña phase. Such characteristic TC density anomalies can be attributed to the steering flow patterns in FLOR and HiFLOR (Fig. 17). Therefore, the responses of the Walker circulation (averaged over 5°–20°N) and steering flow to ENSO in HiFLOR are better simulated than FLOR in the restoring ensemble experiments. Such responses, in addition to the improved simulation of ENSO, contribute to the improved simulation of TC density and genesis in HiFLOR.

4. Discussion and conclusions

ENSO–TC connections in the WNP have attracted tremendous attention over the decades, with analyses based on both observations and dynamic models. Over time, AGCMs and CGCMs have reported large improvements in the simulation of ENSO–TC connections. However, the performance of such simulations is not yet satisfactory because of remaining model biases and gaps in our understanding of ENSO–TC connections.

TABLE 3. Correlation coefficients between TC landfall over Japan and the Korea Peninsula, the Philippines, ICMP, China and East Asia and the Niño-3.4 index based on observations, and the SST-restoring experiments with HiFLOR and FLOR for the period of 1971–2012. Three, two, and one asterisk(s) indicate results that are significant at the levels of 0.01, 0.05, and 0.1, respectively.

TC landfall correlation	IBTrACS	FLOR (SST restoring)	HiFLOR (SST restoring)
Japan and the Korea Peninsula	−0.02	−0.07	−0.16
Philippines	−0.24*	−0.28**	−0.41***
ICMP	−0.30**	−0.12	−0.51***
China	−0.49***	0.32**	−0.38***
East Asia	−0.27**	0.03	−0.61***

Although the GFDL CM 2.5 has shown encouraging results for the responses of TC activity to ENSO, a larger eastward shift and higher magnitude in anomalous TC density in the WNP were found during El Niño and La Niña phases compared to the observations (Kim et al. 2014). FLOR inherits this ENSO–TC association in the WNP from CM2.5 as reported in Vecchi et al. (2014). Recently, GFDL has developed the High-Resolution

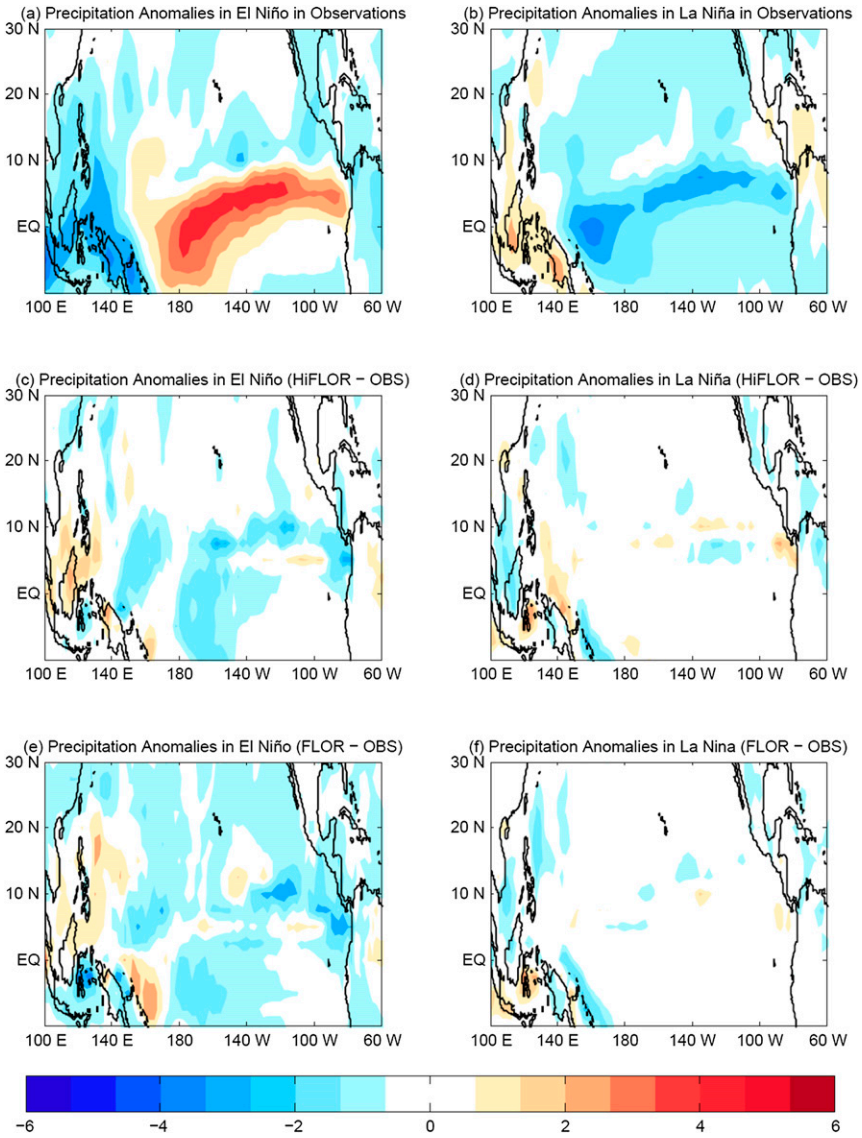

FIG. 15. Precipitation anomalies (mm day^{-1}) during El Niño and La Niña phases based on (a),(b) observations, (c),(d) SST-restoring HiFLOR − observations, and (e),(f) SST-restoring FLOR − observations.

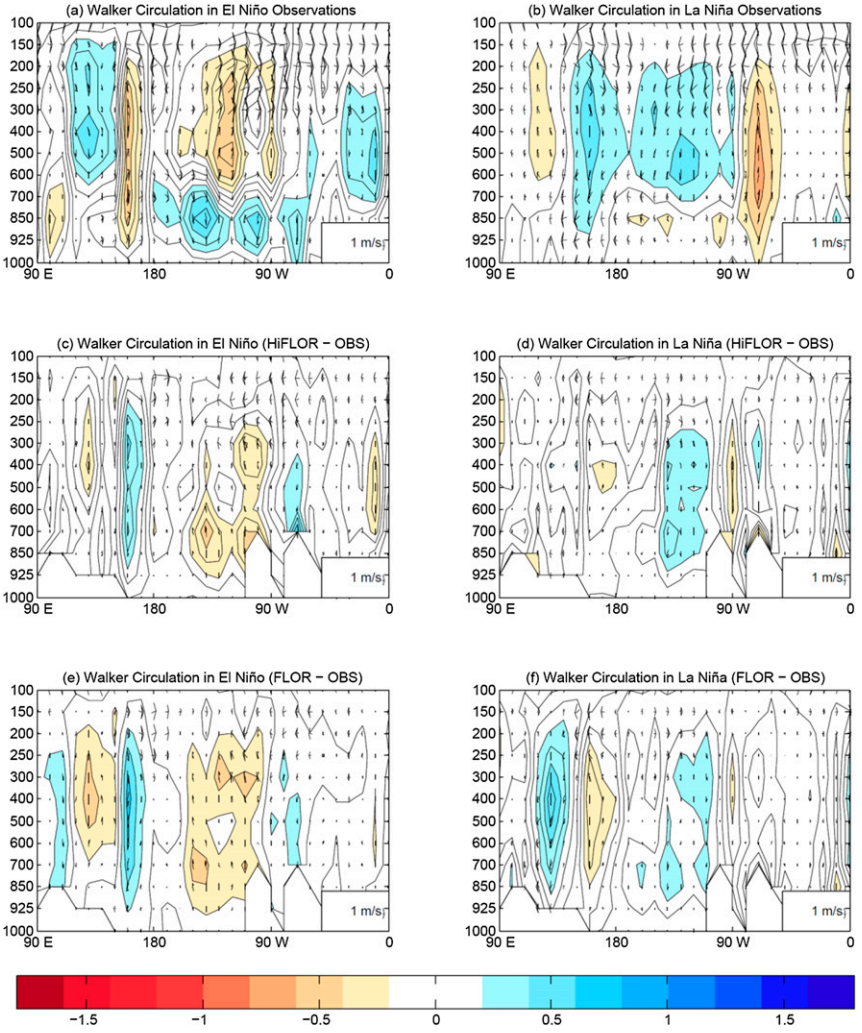

FIG. 16. Vertical profile in pressure (hPa) of wind vectors [zonal wind (averaged over 5°–20°N) and ω scaled by $-50\,\mathrm{Pa\,s^{-1}}$] during El Niño and La Niña phases based on (a),(b) observations, (c),(d) SST-restoring HiFLOR − observations, and (e),(f) SST-restoring FLOR − observations to depict the Walker circulation. The shading represents the unscaled ω.

FLOR (HiFLOR) with a spatial horizontal resolution of 25 km, which performs much better than FLOR in the simulation of global category-4 and category-5 TCs, especially in the North Atlantic (Murakami et al. 2015). This study aims to assess whether and by what mechanisms HiFLOR improves the simulation of ENSO–TC connections in the WNP by using long-term control simulations and restoring ensemble experiments. Our research findings are summarized as follows.

1) HiFLOR simulates better ENSO–TC connections in the WNP including the TC track density, genesis, and landfall than FLOR in both long-term control experiments and SST-restoring historical runs (1971–2012).
2) In the control experiments of HiFLOR, an improved simulation of the Walker circulation related to SST and deep convection is largely responsible for its better performance in simulating ENSO–TC connections in the WNP. In the SST-restoring experiments of HiFLOR, more realistic Walker circulation and steering flow with HiFLOR during El Niño and La Niña are responsible for the better simulation of TC activity in the WNP.
3) An improved simulation of ENSO–TC connections with HiFLOR arises from a better representation of SST and better responses of environmental large-scale circulation to SST anomalies associated with El Niño and La Niña.

Fundamentally, HiFLOR differs from FLOR because a higher spatial resolution of atmospheric and land components. The enhanced resolution of the atmospheric

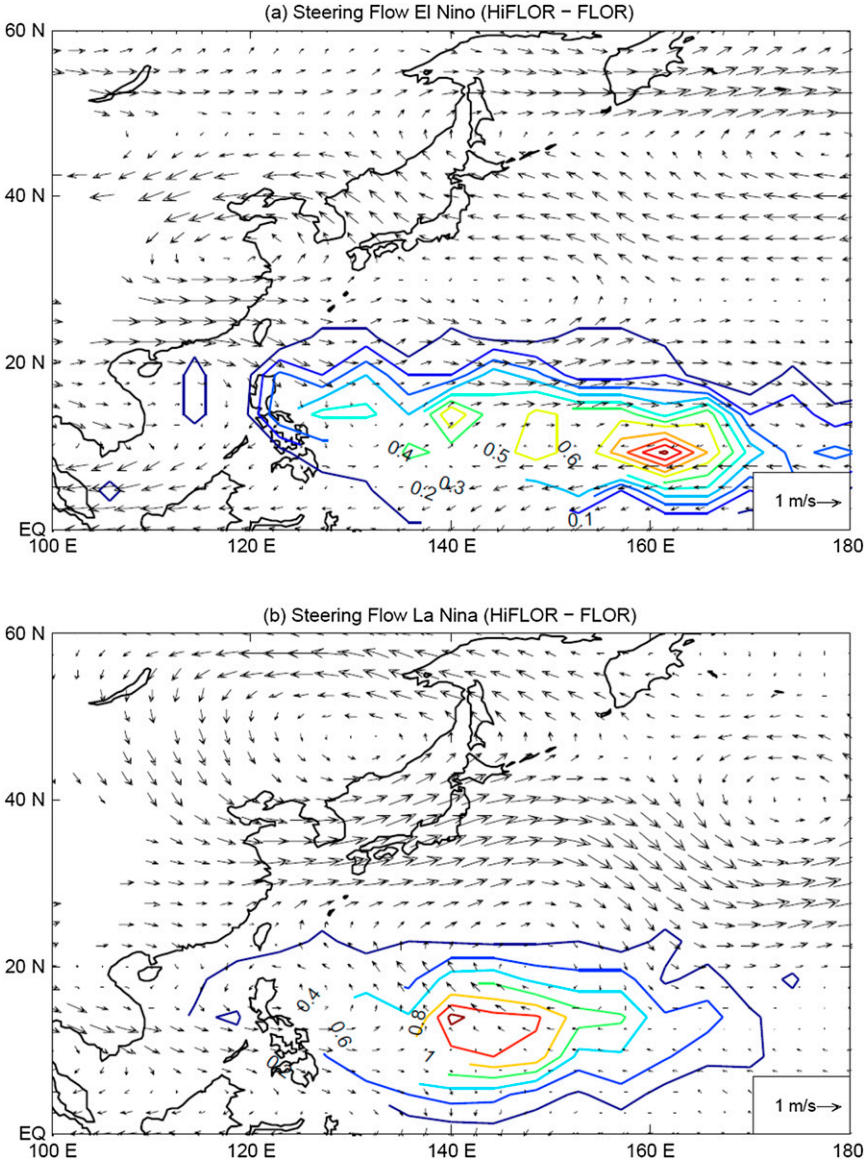

FIG. 17. Steering flow differences (HiFLOR minus FLOR; m s^{-1}) in the SST-restoring experiments during the (a) El Niño and (b) La Niña phase. Contours represent the annual average TC genesis density in HiFLOR.

component in HiFLOR relative to FLOR results in coupled feedback that drives an improved ENSO SST simulation; the SST in turn drives better atmospheric responses in HiFLOR (Murakami et al. 2015). This partly explains the better performance of HiFLOR in simulating ENSO–TC connections in the WNP. However, as demonstrated in the SST-restored experiments, even with the very similar SSTs HiFLOR outperforms FLOR in WNP TCs. Using a CGCM with a horizontal resolution of 60 km, the simulated TC genesis is shifted more eastward during La Niña years in contrast to the observations (Iizuka and Matsuura 2008). Bell et al. (2014) showed that both the High-Resolution Global Environmental Model (HiGEM) and its atmosphere-only component (HiGAM) produce encouraging simulations of global ENSO–TC connections. However, large negative (positive) TC track density anomalies are simulated in the western WNP during El Niño and La Niña phases (Bell et al. 2014). This may arise from the different months selected for TC density analysis because the current study analyzed TC from July to October while Bell et al. (2014) examined TCs from May to November or from model biases. The current study has shown that HiFLOR performed better than FLOR in simulating ENSO–TC connections in terms

of genesis and track and landfall in the WNP. HiFLOR produces simulations comparable to or slightly better than other models and the better simulation with HiFLOR is largely attributed to the more realistic representation of SST and the improved large-scale circulation responses to El Niño and La Niña associated with SST anomalies.

Although this study has shown encouraging results for ENSO–TC connections based on state-of-the-art HiFLOR and FLOR, we still need further improvements in the simulation of total TC genesis in the WNP. This is particularly true for the areas with strong TC density anomalies around the East Asian coast and the Philippine Sea in HiFLOR. A better representation of ENSO–TC connections may benefit the seasonal forecasting of TC genesis, track, and landfall, improve our understanding of the interannual variation of TC activity and provide better projection of TC activity under climate change. Such analysis will be conducted in our future studies. Because an improved simulation of ENSO–TC connections in the WNP is also observed in SST-restoring experiments, it is thus of great interest to examine whether or not HiFLOR can outperform FLOR in seasonal forecasting of WNP TC activity.

Acknowledgments. The authors thank the editor and three anonymous reviewers for insightful comments and suggestions. The authors are grateful to Lakshmi Krishnamurti and Liping Zhang for their valuable comments on an earlier version of this paper. The authors thank Fanrong Zeng for helpful assistance in experiments. This material is based in part upon work supported by the National Science Foundation under Grants AGS-1262091 and AGS-1262099.

APPENDIX

Tracking Algorithm

The tracker is developed by L. Harris et al. (unpublished manuscript) to track TCs from 6-h climate simulations. This tracker was also employed in Zhang et al. (2016) and Murakami et al. (2015). The tracking processes are based on key variables such as temperature, sea level pressure (SLP), and 10-m wind. The tracking procedures are described as follows.

1) Local minima of the smoothed SLP field are found. The location of the center is properly adjusted by fitting a biquadratic function to the SLP and locating the center at the minimum.
2) Closed contours in an interval of 2 hPa ($=dp$) around every single SLP low center. The Nth contour is marked as the contiguous region surrounding a low central pressure P with pressures lower than $Ndp + P$, as detected by a "flood fill" algorithm. It is noted that the contours are not required to be circular and a maximum radius of 3000 km will be searched from each candidate low center.
3) If the algorithm detects contours that are close enough, the low is counted in as a TC center. In this way, the tracker attempts to find all closed contours in the vicinity of the low center within a certain distance from the low center and without entering contours belonging to another low. The maximum 10-m wind inside the set of closed contours is taken as the maximum wind speed at that time for the storm.
4) Warm cores are detected via similar processes: closed 1°C contours for FLOR are found surrounding the maximum temperature anomaly (t_a) within a TC's identified contours, no more than 1° from the low center. This contour must have a radius smaller than 3° in distance. If there is not such a core, it should not be marked as a warm-core low center, although the center is not rejected.
5) TC centers are combined into a track by taking a low center at time $T - dt$, extrapolating its motion forward dt, and then seeking storms within 750 km. It is noted that a deeper low center has higher priority of tracking.
6) The following criteria are required to pick up the final TCs:
   (i) at least 72 h of total detection lifetime (not necessarily consecutive),
   (ii) at least 48 cumulative (not necessarily consecutive) hours with a warm core,
   (iii) at least 36 consecutive hours of a warm core with winds greater than 17.5 m s^{-1}, and
   (iv) TC genesis should be confined equatorward of 40°N.

REFERENCES

Adler, R. F., and Coauthors, 2003: The version-2 Global Precipitation Climatology Project (GPCP) monthly precipitation analysis (1979–present). *J. Hydrometeor.*, **4**, 1147–1167, doi:10.1175/1525-7541(2003)004<1147:TVGPCP>2.0.CO;2.

Alexander, M. A., I. Bladé, M. Newman, J. R. Lanzante, N.-C. Lau, and J. D. Scott, 2002: The atmospheric bridge: The influence of ENSO teleconnections on air–sea interaction over the global oceans. *J. Climate*, **15**, 2205–2231, doi:10.1175/1520-0442(2002)015<2205:TABTIO>2.0.CO;2.

Antonov, J. I., R. A. Locarnini, T. P. Boyer, A. V. Mishonov, and H. E. Garcia, 2006: *Salinity*. Vol. 2, *World Ocean Atlas 2005*, NOAA Atlas NESDIS 62, 182 pp.

Bell, R., K. Hodges, P. L. Vidale, J. Strachan, and M. Roberts, 2014: Simulation of the global ENSO–tropical cyclone teleconnection by a high-resolution coupled general circulation model. *J. Climate*, **27**, 6404–6422, doi:10.1175/JCLI-D-13-00559.1.

Camargo, S. J., and A. H. Sobel, 2005: Western North Pacific tropical cyclone intensity and ENSO. *J. Climate*, **18**, 2996–3006, doi:10.1175/JCLI3457.1.

——, A. G. Barnston, and S. E. Zebiak, 2005: A statistical assessment of tropical cyclone activity in atmospheric general circulation models. *Tellus*, **57A**, 589–604, doi:10.1111/j.1600-0870.2005.00117.x.

——, A. W. Robertson, S. J. Gaffney, P. Smyth, and M. Ghil, 2007: Cluster analysis of typhoon tracks. Part II: Large-scale circulation and ENSO. *J. Climate*, **20**, 3654–3676, doi:10.1175/JCLI4203.1.

Cane, M. A., and S. E. Zebiak, 1985: A theory for El Niño and the Southern Oscillation. *Science*, **228**, 1085–1087, doi:10.1126/science.228.4703.1085.

Chan, J. C. L., 1985: Tropical cyclone activity in the northwest Pacific in relation to the El Niño/Southern Oscillation phenomenon. *Mon. Wea. Rev.*, **113**, 599–606, doi:10.1175/1520-0493(1985)113<0599:TCAITN>2.0.CO;2.

——, 2000: Tropical cyclone activity over the western North Pacific associated with El Niño and La Niña events. *J. Climate*, **13**, 2960–2972, doi:10.1175/1520-0442(2000)013<2960:TCAOTW>2.0.CO;2.

——, 2008: Decadal variations of intense typhoon occurrence in the western North Pacific. *Proc. Roy. Soc.*, **464A**, 249–272, doi:10.1098/rspa.2007.0183.

——, and X. Liang, 2003: Convective asymmetries associated with tropical cyclone landfall. Part I: *f*-plane simulations. *J. Atmos. Sci.*, **60**, 1560–1576, doi:10.1175/1520-0469(2003)60<1560:CAAWTC>2.0.CO;2.

——, and K. S. Liu, 2004: Global warming and western North Pacific typhoon activity from an observational perspective. *J. Climate*, **17**, 4590–4602, doi:10.1175/3240.1.

——, and M. Xu, 2009: Interannual and inter-decadal variations of landfalling tropical cyclones in East Asia. Part I: Time series analysis. *Int. J. Climatol.*, **29**, 1285–1293.

——, Y. H. Duan, and L. K. Shay, 2001: Tropical cyclone intensity change from a simple ocean–atmosphere coupled model. *J. Atmos. Sci.*, **58**, 154–172, doi:10.1175/1520-0469(2001)058<0154:TCICFA>2.0.CO;2.

Chen, G., and C.-Y. Tam, 2010: Different impacts of two kinds of Pacific Ocean warming on tropical cyclone frequency over the western North Pacific. *Geophys. Res. Lett.*, **37**, L01803, doi:10.1029/2009GL041708.

Chen, J.-H., and S.-J. Lin, 2011: The remarkable predictability of interannual variability of Atlantic hurricanes during the past decade. *Geophys. Res. Lett.*, **38**, L11804, doi:10.1029/2011GL047629.

——, and ——, 2013: Seasonal predictions of tropical cyclones using a 25-km-resolution general circulation model. *J. Climate*, **26**, 380–398, doi:10.1175/JCLI-D-12-00061.1.

Chia, H. H., and C. Ropelewski, 2002: The interannual variability in the genesis location of tropical cyclones in the northwest Pacific. *J. Climate*, **15**, 2934–2944, doi:10.1175/1520-0442(2002)015<2934:TIVITG>2.0.CO;2.

Chiang, J. C. H., and B. R. Lintner, 2005: Mechanisms of remote tropical surface warming during El Niño. *J. Climate*, **18**, 4130–4149, doi:10.1175/JCLI3529.1.

Dawson, A., A. J. Matthews, D. P. Stevens, M. J. Roberts, and P. L. Vidale, 2013: Importance of oceanic resolution and mean state on the extra-tropical response to El Niño in a matrix of coupled models. *Climate Dyn.*, **41**, 1439–1452, doi:10.1007/s00382-012-1518-6.

Delworth, T. L., and Coauthors, 2012: Simulated climate and climate change in the GFDL CM2.5 high-resolution coupled climate model. *J. Climate*, **25**, 2755–2781, doi:10.1175/JCLI-D-11-00316.1.

Dobos, P. H., and R. L. Elsberry, 1993: Forecasting tropical cyclone recurvature. Part I: Evaluation of existing methods. *Mon. Wea. Rev.*, **121**, 1273–1278, doi:10.1175/1520-0493(1993)121<1273:FTCRPI>2.0.CO;2.

Dvorak, V. F., 1984: Tropical cyclone intensity analysis using satellite data. NOAA Tech. Rep. NESDIS 11, 47 pp.

Emanuel, K., 2005: *Divine Wind: The History and Science of Hurricanes*. Oxford University Press, 296 pp.

——, C. DesAutels, C. Holloway, and R. Korty, 2004: Environmental control of tropical cyclone intensity. *J. Atmos. Sci.*, **61**, 843–858, doi:10.1175/1520-0469(2004)061<0843:ECOTCI>2.0.CO;2.

Fraedrich, K., and L. M. Leslie, 1989: Estimates of cyclone track predictability. I: Tropical cyclones in the Australian region. *Quart. J. Roy. Meteor. Soc.*, **115**, 79–92, doi:10.1002/qj.49711548505.

Fu, B., M. S. Peng, T. Li, and D. E. Stevens, 2012: Developing versus nondeveloping disturbances for tropical cyclone formation. Part II: Western North Pacific. *Mon. Wea. Rev.*, **140**, 1067–1080, doi:10.1175/2011MWR3618.1.

Fudeyasu, H., S. Iizuka, and T. Matsuura, 2006: Impact of ENSO on landfall characteristics of tropical cyclones over the western North Pacific during the summer monsoon season. *Geophys. Res. Lett.*, **33**, L21815, doi:10.1029/2006GL027449.

George, J. E., and W. M. Gray, 1977: Tropical cyclone recurvature and nonrecurvature as related to surrounding wind–height fields. *J. Appl. Meteor.*, **16**, 34–42, doi:10.1175/1520-0450(1977)016<0034:TCRANA>2.0.CO;2.

Gray, W. M., 1979: Hurricanes: Their formation, structure and likely role in the tropical circulation. *Meteorology over the Tropical Oceans*, D. B. Shaw, Ed., Royal Meteorological Society, 155–218.

——, 1998: The formation of tropical cyclones. *Meteor. Atmos. Phys.*, **67**, 37–69, doi:10.1007/BF01277501.

Harr, P. A., and R. L. Elsberry, 1991: Tropical cyclone track characteristics as a function of large-scale circulation anomalies. *Mon. Wea. Rev.*, **119**, 1448–1468, doi:10.1175/1520-0493(1991)119<1448:TCTCAA>2.0.CO;2.

Holland, G. J., and M. Lander, 1993: The meandering nature of tropical cyclone tracks. *J. Atmos. Sci.*, **50**, 1254–1266, doi:10.1175/1520-0469(1993)050<1254:TMNOTC>2.0.CO;2.

Hong, C.-C., Y.-H. Li, T. Li, and M.-Y. Lee, 2011: Impacts of central Pacific and eastern Pacific El Niños on tropical cyclone tracks over the western North Pacific. *Geophys. Res. Lett.*, **38**, L16712, doi:10.1029/2011GL048821.

Iizuka, S., and T. Matsuura, 2008: ENSO and western North Pacific tropical cyclone activity simulated in a CGCM. *Climate Dyn.*, **30**, 815–830, doi:10.1007/s00382-007-0326-x.

Jia, L., and Coauthors, 2015: Improved seasonal prediction of temperature and precipitation over land in a high-resolution GFDL climate model. *J. Climate*, **28**, 2044–2062, doi:10.1175/JCLI-D-14-00112.1.

Kalnay, E., and Coauthors, 1996: The NCEP/NCAR 40-Year Reanalysis Project. *Bull. Amer. Meteor. Soc.*, **77**, 437–471, doi:10.1175/1520-0477(1996)077<0437:TNYRP>2.0.CO;2.

Kim, H.-M., P. J. Webster, and J. A. Curry, 2009: Impact of shifting patterns of Pacific Ocean warming on North Atlantic tropical cyclones. *Science*, **325**, 77–80, doi:10.1126/science.1174062.

Kim, H.-S., G. A. Vecchi, T. R. Knutson, W. G. Anderson, T. L. Delworth, A. Rosati, F. Zeng, and M. Zhao, 2014: Tropical cyclone simulation and response to CO_2 doubling in the GFDL CM2.5 high-resolution coupled climate model. *J. Climate*, **27**, 8034–8054, doi:10.1175/JCLI-D-13-00475.1.

Kirtman, B. P., and Coauthors, 2014: The North American multimodel ensemble: Phase-1 seasonal-to-interannual prediction; phase-2 toward developing intraseasonal prediction. *Bull. Amer. Meteor. Soc.*, **95**, 585–601, doi:10.1175/BAMS-D-12-00050.1.

Knapp, K. R., M. C. Kruk, D. H. Levinson, H. J. Diamond, and C. J. Neumann, 2010: The International Best Track Archive for Climate Stewardship (IBTrACS). *Bull. Amer. Meteor. Soc.*, **91**, 363–376, doi:10.1175/2009BAMS2755.1.

Kobayashi, S., and Coauthors, 2015: The JRA-55 Reanalysis: General specifications and basic characteristics. *J. Meteor. Soc. Japan*, **93**, 5–48, doi:10.2151/jmsj.2015-001.

Krishnamurthy, L., G. Vecchi, R. Msadek, A. Wittenberg, T. Delworth, and F. Zeng, 2015: The seasonality of the Great Plains low-level jet and ENSO relationship. *J. Climate*, **28**, 4525–4544, doi:10.1175/JCLI-D-14-00590.1.

——, ——, ——, H. Murakami, A. Wittenberg, and F. Zeng, 2016: Impact of strong ENSO on regional tropical cyclone activity in a high-resolution climate model in the North Pacific and North Atlantic Oceans. *J. Climate*, doi: 10.1175/JCLI-D-15-0468.1, in press.

Lau, K.-M., and S. Yang, 1996: Seasonal variation, abrupt transition, and intraseasonal variability associated with the Asian summer monsoon in the GLA GCM. *J. Climate*, **9**, 965–985, doi:10.1175/1520-0442(1996)009<0965:SVATAI>2.0.CO;2.

Lau, N.-C., and M. J. Nath, 1996: The role of the ''atmospheric bridge'' in linking tropical Pacific ENSO events to extratropical SST anomalies. *J. Climate*, **9**, 2036–2057, doi:10.1175/1520-0442(1996)009<2036:TROTBI>2.0.CO;2.

Li, C., and C. Wang, 2014: Simulated impacts of two types of ENSO events on tropical cyclone activity in the western North Pacific: Large-scale atmospheric response. *Climate Dyn.*, **42**, 2727–2743, doi:10.1007/s00382-013-1999-y.

Li, R. C., and W. Zhou, 2012: Changes in western Pacific tropical cyclones associated with the El Niño–Southern Oscillation cycle. *J. Climate*, **25**, 5864–5878, doi:10.1175/JCLI-D-11-00430.1.

Lyons, S. W., 2004: U.S. tropical cyclone landfall variability: 1950–2002. *Wea. Forecasting*, **19**, 473–480, doi:10.1175/1520-0434(2004)019<0473:UTCLV>2.0.CO;2.

Magnusson, L., M. Alonso-Balmaseda, and F. Molteni, 2013: On the dependence of ENSO simulation on the coupled model mean state. *Climate Dyn.*, **41**, 1509–1525, doi:10.1007/s00382-012-1574-y.

Msadek, R., G. A. Vecchi, M. Winton, and R. G. Gudgel, 2014: Importance of initial conditions in seasonal predictions of Arctic sea ice extent. *Geophys. Res. Lett.*, **41**, 5208–5215, doi:10.1002/2014GL060799.

Murakami, H., and M. Sugi, 2010: Effect of model resolution on tropical cyclone climate projections. *SOLA*, **6**, 73–76, doi:10.2151/sola.2010-019.

——, and B. Wang, 2010: Future change of North Atlantic tropical cyclone tracks: Projection by a 20-km-mesh global atmospheric model. *J. Climate*, **23**, 2699–2721, doi:10.1175/2010JCLI3338.1.

——, ——, and A. Kitoh, 2011: Future change of western North Pacific typhoons: Projections by a 20-km-mesh global atmospheric model. *J. Climate*, **24**, 1154–1169, doi:10.1175/2010JCLI3723.1.

——, and Coauthors, 2015: Simulation and prediction of category 4 and 5 hurricanes in the high-resolution GFDL HiFLOR coupled climate model. *J. Climate*, **28**, 9058–9079, doi:10.1175/JCLI-D-15-0216.1.

Peduzzi, P., B. Chatenoux, H. Dao, A. De Bono, C. Herold, J. Kossin, F. Mouton, and O. Nordbeck, 2012: Global trends in tropical cyclone risk. *Nat. Climate Change*, **2**, 289–294, doi:10.1038/nclimate1410.

Philander, S. G. H., 1983: El Niño Southern Oscillation phenomena. *Nature*, **302**, 295–301, doi:10.1038/302295a0.

Pielke, R., Jr., J. Gratz, C. Landsea, D. Collins, M. Saunders, and R. Musulin, 2008: Normalized hurricane damage in the United States: 1900–2005. *Nat. Hazards Rev.*, **9**, 29–42, doi:10.1061/(ASCE)1527-6988(2008)9:1(29).

Rasmusson, E. M., and T. H. Carpenter, 1982: Variations in tropical sea surface temperature and surface wind fields associated with the Southern Oscillation/El Niño. *Mon. Wea. Rev.*, **110**, 354–384, doi:10.1175/1520-0493(1982)110<0354:VITSST>2.0.CO;2.

Rayner, N., D. E. Parker, E. Horton, C. Folland, L. Alexander, D. Rowell, E. Kent, and A. Kaplan, 2003: Global analyses of sea surface temperature, sea ice, and night marine air temperature since the late nineteenth century. *J. Geophys. Res.*, **108**, 4407, doi:10.1029/2002JD002670.

Riehl, H., and R. J. Shafer, 1944: The recurvature of tropical storms. *J. Atmos. Sci.*, **1**, 42–54, doi:10.1175/1520-0469(1944)001<0001:TROTS>2.0.CO;2.

Shaevitz, D. A., and Coauthors, 2014: Characteristics of tropical cyclones in high-resolution models in the present climate. *J. Adv. Model. Earth Syst.*, **6**, 1154–1172, doi:10.1002/2014MS000372.

Shaffrey, L. C., and Coauthors, 2009: UK HiGEM: The new UK high-resolution global environment model—Model description and basic evaluation. *J. Climate*, **22**, 1861–1896, doi:10.1175/2008JCLI2508.1.

Trenberth, K. E., J. M. Caron, D. P. Stepaniak, and S. Worley, 2002: Evolution of El Niño–Southern Oscillation and global atmospheric surface temperatures. *J. Geophys. Res.*, **107**, doi:10.1029/2000JD000298.

Tuleya, R., M. Bender, and Y. Kurihara, 1984: A simulation study of the landfall of tropical cyclones using a movable nested-mesh model. *Mon. Wea. Rev.*, **112**, 124–136, doi:10.1175/1520-0493(1984)112<0124:ASSOTL>2.0.CO;2.

Vecchi, G. A., and Coauthors, 2014: On the seasonal forecasting of regional tropical cyclone activity. *J. Climate*, **27**, 7994–8016, doi:10.1175/JCLI-D-14-00158.1.

Vitart, F., and J. Anderson, 2001: Sensitivity of Atlantic tropical storm frequency to ENSO and interdecadal variability of SSTs in an ensemble of AGCM integrations. *J. Climate*, **14**, 533–545, doi:10.1175/1520-0442(2001)014<0533:SOATSF>2.0.CO;2.

Wang, B., and J. C. L. Chan, 2002: How strong ENSO events affect tropical storm activity over the western North Pacific. *J. Climate*, **15**, 1643–1658, doi:10.1175/1520-0442(2002)015<1643:HSEEAT>2.0.CO;2.

Wang, H., J. Sun, and K. Fan, 2007: Relationships between the North Pacific Oscillation and the typhoon/hurricane frequencies. *Sci. China*, **50D**, 1409–1416, doi:10.1007/s11430-007-0097-6.

——, and Coauthors, 2014: How well do global climate models simulate the variability of Atlantic tropical cyclones associated with ENSO? *J. Climate*, **27**, 5673–5692, doi:10.1175/JCLI-D-13-00625.1.

Wong, M. L. M., and J. C. L. Chan, 2004: Tropical cyclone intensity in vertical wind shear. *J. Atmos. Sci.*, **61**, 1859–1876, doi:10.1175/1520-0469(2004)061<1859:TCIIVW>2.0.CO;2.

Wu, G., and N.-C. Lau, 1992: A GCM simulation of the relationship between tropical-storm formation and ENSO. *Mon. Wea. Rev.*, **120**, 958–977, doi:10.1175/1520-0493(1992)120<0958:AGSOTR>2.0.CO;2.

Wu, L., and B. Wang, 2000: A potential vorticity tendency diagnostic approach for tropical cyclone motion. *Mon. Wea.*

Rev., **128**, 1899–1911, doi:10.1175/1520-0493(2000)128<1899:APVTDA>2.0.CO;2.

——, and ——, 2001: Movement and vertical coupling of adiabatic baroclinic tropical cyclones. *J. Atmos. Sci.*, **58**, 1801–1814, doi:10.1175/1520-0469(2001)058<1801:MAVCOA>2.0.CO;2.

Wu, M., W. Chang, and W. Leung, 2004: Impacts of El Niño–Southern Oscillation events on tropical cyclone landfalling activity in the western North Pacific. *J. Climate*, **17**, 1419–1428, doi:10.1175/1520-0442(2004)017<1419:IOENOE>2.0.CO;2.

Wunsch, C., 1991: Large-scale response of the ocean to atmospheric forcing at low frequencies. *J. Geophys. Res.*, **96**, 15 083–15 092, doi:10.1029/91JC01457.

Yang, X., and Coauthors, 2015a: Seasonal predictability of extratropical storm tracks in GFDL's high-resolution climate prediction model. *J. Climate*, **28**, 3592–3611, doi:10.1175/JCLI-D-14-00517.1.

——, G. A. Vecchi, T. L. Delworth, K. Paffendorf, R. Gudgel, L. Jia, S. D. Underwood, and F. Zeng, 2015b: Extreme North America winter storm season of 2013/14: Roles of radiative forcing and the global warming hiatus [in ''Explaining Extremes of 2014 from a Climate Perspective'']. *Bull. Amer. Meteor. Soc.*, S25–S28, doi:10.1175/BAMS-D-15-00133.

Zehr, R. M., 1992: Tropical cyclogenesis in the western North Pacific. Ph.D. thesis, Colorado State University, 181 pp.

Zhang, Q., Q. Liu, and L. Wu, 2009: Tropical cyclone damages in China 1983–2006. *Bull. Amer. Meteor. Soc.*, **90**, 489–495, doi:10.1175/2008BAMS2631.1.

Zhang, W., H. F. Graf, Y. Leung, and M. Herzog, 2012: Different El Niño types and tropical cyclone landfall in East Asia. *J. Climate*, **25**, 6510–6523, doi:10.1175/JCLI-D-11-00488.1.

——, Y. Leung, and K. Fraedrich, 2015: Different El Niño types and intense typhoons in the western North Pacific. *Climate Dyn.*, **44**, 2965–2977, doi:10.1007/s00382-014-2446-4.

——, G. Vecchi, H. Murakami, G. Villarini, and L. Jia, 2016: The Pacific meridional mode and the occurrence of tropical cyclones in the western North Pacific. *J. Climate*, **29**, 381–398, doi:10.1175/JCLI-D-15-0282.1.

Zhao, M., I. M. Held, S.-J. Lin, and G. A. Vecchi, 2009: Simulations of global hurricane climatology, interannual variability, and response to global warming using a 50-km resolution GCM. *J. Climate*, **22**, 6653–6678, doi:10.1175/2009JCLI3049.1.

——, ——, and G. A. Vecchi, 2010: Retrospective forecasts of the hurricane season using a global atmospheric model assuming persistence of SST anomalies. *Mon. Wea. Rev.*, **138**, 3858–3868, doi:10.1175/2010MWR3366.1.